nagra National Cooperative for the Disposal of Radioactive Waste

TECHNICAL REPORT 93-16

Propagation of a Hyperalkaline Plume into the Geological Barrier Surrounding a Radioactive Waste Repository

July 1994

P.C. Lichtner
J. Eikenberg

Hardstrasse 73, CH-5430 Wettingen/Switzerland, Telephone +41-56-37 11 11

nagra National Cooperative for the Disposal of Radioactive Waste

TECHNICAL REPORT 93-16

Propagation of a Hyperalkaline Plume into the Geological Barrier Surrounding a Radioactive Waste Repository

July 1994

P.C. Lichtner [1)]
J. Eikenberg [2)]

1) Geologisches und Mineralogisch-petrographisches Institut, Universität Bern

2) PSI, Würenlingen and Villigen

Hardstrasse 73, CH-5430 Wettingen/Switzerland, Telephone +41-56-37 11 11

This report was prepared on behalf of Nagra. The viewpoints presented and conclusions reached are those of the author(s) and do not necessarily represent those of Nagra.

Preface

In the framework of its Waste Management Programme the Paul Scherrer Institute is performing work to increase the understanding of repository near-field behaviour. These investigations are performed in close cooperation with, and with the financial support of NAGRA. The present report is issued simultaneously as a PSI Report and NAGRA NTB 93-16.

ABSTRACT

A probable consequence of siting a cement-based low- and intermediate-level radioactive waste repository in a marl host rock is the release of a hyperalkaline plume with initial pH values as high as 13 or greater, resulting in aggressive alteration of the surrounding host rock. Thermodynamic stability relations indicate that various rock-forming silicate minerals are unstable in strongly alkaline solutions, and therefore significant alteration of the physical and chemical properties of the host rock is likely. Because of the low silica concentration characteristic of Portland cement pore fluid, a silicate-bearing host rock will dissolve on initial contact with the hyperalkaline plume. The duration of the plume could be tenthousands of years or more, depending on the amount of cement in the repository. A coupled geochemical transport model (MPATH) which includes chemical reaction kinetics is used to evaluate the alteration of Swiss argillaceous sediments in a high-pH environment and to predict the spatial propagation of the hyperalkaline plume with time. The calculations predict dissolution of quartz, clay minerals and chlorite, and precipitation of zeolite minerals such as analcime and natrolite as well as the feldspars K-feldspar and albite. In addition, Portland cement-hydrates such as calcium silicate and aluminate hydrates, ettringite and friedel-salt are also predicted to form, depending on the composition of the inlet fluid and the host rock. The dissolution of clay minerals reduces the pH of the hyperalkaline plume to levels between approximately 8 and 10, depending on the composition of the inlet fluid and the host rock. For pure advective transport through a porous medium, neglecting changes in porosity and permeability, the migration velocity of the high-pH front is calculated to be approximately one to two orders of magnitude less than that of the infiltrating groundwater. However, due to precipitation of secondary phases, in the present model concept a rapid decrease in porosity of the marl occurs several meters from the repository. At the interface between the marl host rock and cement the porosity increases as a consequence of the low silica concentration of the cement pore fluid.

ZUSAMMENFASSUNG

Das Endlager SMA besteht vor allem aus Beton. Das Porenwasser in Beton ist stark alkalisch (pH > 13 bei Endlagerverschluss). Aus dem Endlager austretendes Betonporenwasser ist nicht im Gleichgewicht mit Valanginienmergel, der als Wirtgestein für das Endlager SMA vorgesehen ist. Thermodynamische Stabilitätsbeziehungen weisen darauf hin, dass verschiedene Mineralkomponenten von Valanginienmergel unter stark alkalischen Bedingungen instabil sind und daher eine signifikante Veränderung der chemischen und physikalischen Eigenschaften von Valanginienmergel zu erwarten sind. Wegen den tiefen Siliziumkonzentrationen des Betonporenwassers lösen sich silikathaltige Mineralkomponenten von Mergel in Kontakt mit Betonporenwasser auf. Die Umwandlungsdauer des Wirtgesteins kann sich über zehntausende von Jahren erstrecken und ist von der Betonmenge im Endlager SMA abhängig. Im vorliegenden Bericht wird das Rechenprogramm MPATH, das advektiven Transport mit chemischen Reaktionen koppelt, angewendet, um die Alterierung von Valanginienmergel durch Betonporenwasser in Abhängigkeit des Ortes und der Zeit zu modellieren. Die Modellierungen sagen voraus, dass die meisten gesteinsbildenden Mineralien des Mergel (Quartz, Chlorit, Tonmineralien) aufgelöst werden und an ihrer Stelle Zeolithe, Feldspäte und zementartige Mineralien gebildet werden. Durch die Auflösung der Tonmineralien wird der pH des infiltrierenden Betonporenwassers auf Werte zwischen 8 und 10 reduziert. Ohne Berücksichtigung von Porositäts- und Permeabilitätsänderungen ist die Ausbreitungsgeschwindigkeit der pH-Front in einem porösen Medium ein bis zwei Grössenordnungen kleiner als die Migrationsgeschwindigkeit des infiltrierenden Grundwassers. An der Grenzfläche Beton zu Mergel wird die Porosität erhöht, bedingt durch die geringen Siliziumkonzentrationen des Betonporenwassers; im Abstand von eingen Metern wird die Porosität verkleinert, durch die Ausfällung von Sekundärfestphasen.

RESUME

Une conséquence probable de l'implantation d'un dépôt final pour déchets de faible et moyenne activité dans une formation de marnes valanginiennes sera le relâchement d'un panache hyperalcalin dont les valeurs initiales de pH pourraient atteindre 13 ou plus, entraînant une altération agressive de la roche d'accueil environnante. Des relations de stabilité thermodynamique indiquent que divers minéraux de silicates constituant les roches sont instables dans des solutions fortement alcalines; des altérations significatives des propriétés physiques et chimiques de la roche d'accueil sont par conséquent vraisemblables. En raison de la faible concentration de silice, typique du fluide intersticiel des ciments Portland, une roche d'accueil comportant des silicates doit être dissoute au contact initial avec le panache hyperalcalin. La durée d'existence de ce panache pourrait atteindre des dizaines de milliers d'années, voire davantage, selon la quantité de ciment contenue dans le dépôt final. Un modèle géochimique de transport (MPATH), qui comprend la cinétique de réactions chimiques, est utilisé pour évaluer les altérations de marnes valanginiennes soumises à un environnement de pH élevé et pour prédire la propagation spatiale du panache hyperalcalin en fonction du temps. Les calculs prédisent la dissolution du quartz, de minéraux argileux et de la chlorite ainsi que la précipitation de minéraux du groupe des zéolites tels que l'analcime et la natrolite comme de minéraux siliceux feldspath-K et albite. Selon la composition du fluide intrusif et de la roche d'accueil, on prédit en outre la formation d'hydrates de ciment Portland tels que des silicates de calcium et des hydrates d'aluminates en plus d'ettringite et de sel de friedel. La dissolution de minéraux argileux réduit le pH du panache hyperalcalin à des niveaux situés entre 8 et 10 selon la composition du fluide intrusif et de la roche d'accueil. Pour un transport purement advectif à travers un milieu poreux, négligeant les modifications de porosité et de perméabilité, on calcule une vitesse de migration du front de fort pH d'environ un à deux ordres de grandeur en-dessous de celle de l'eau d'infiltration souterraine. En raison de la précipitation de phases secondaires, une rapide diminution de la porosité de la marne se manifeste toutefois à plusieurs mètres du dépôt. La porosité augmente à l'interface entre la roche d'accueil marneuse et le ciment en raison de la faible concentration de silice dans le fluide intersticiel du ciment.

Contents

ABSTRACT i

ZUSAMMENFASSUNG ii

RESUME iii

LIST OF CONTENTS iv

LIST OF TABLES vi

LIST OF FIGURES vii

1 INTRODUCTION 1

2 GEOCHEMICAL CHARACTERIZATION OF THE CEMENT AND MARL SYSTEMS 3

2.1 Cement Composition 3

2.2 Marl Composition 9

3 INTERACTION OF ROCK WITH HYPERALKALINE FLUIDS 12

3.1 Alkaline Flooding 12

3.2 Alkali and Calcium Hydroxide Titration Experiments 14

3.3 Natural Analogues 15

3.4 Importance of Cation Exchange and Clay Dissolution Reactions 17

4 PHASE EQUILIBRIA AND pH–CONTROLS 19

5 NUMERICAL CALCULATION OF MARL ALTERATION 24

5.1 Time-Space Continuum Model of Mass Transport 25

5.2 Kinetic Formulation of Mineral Reaction Rates 27

5.2.1 Scaling Relations 28

5.2.2 Homogeneous and Fractured Porous Medium 29

5.3 Physicochemical Input Parameters 30

5.3.1 Cement Pore Water Inlet Composition 30

5.3.2 Alkali Release 32

5.3.3 Mineralogical Composition of Marl 34

5.3.4 Flow Conditions 34

5.3.5 Thermodynamic and Kinetic Data 34

5.4 Results 36

5.4.1 pH-Front Propagation 36

5.4.2 Mineralogical Changes Along Flow Path 37

5.4.3 Porosity Changes Along Flow Path 40

5.4.4 Fluid Composition Changes Along Flow Path 42

5.4.5 Alkali Release 43

5.4.6 Sensitivity to Kinetic Rate Constants 45

6 DISCUSSION 47

7 SUMMARY AND CONCLUSION 49

8 ACKNOWLEDGMENTS 50

9 REFERENCES 52

List of Tables

1 Composition of Sulfacem weight percent dry material (taken from Berner, 1990, Table 4). 5

2 Comparison of equilibrium constants for CSH-type phases fitted to experimental solubility data and taken from the EQ3/6 data base. 7

3 Modal composition [vol %] of the marl rock type considered in this study. . . . 10

4 Chemical composition of two marl groundwater types from the Wellenberg region [mol l^{-1}]. 11

5 Stoichiometric coefficients for H^+ for mineral reactions written in terms of the species $Al(OH)_4^-$ and $H_3SiO_4^-$ (n'_H), and Al^{3+} and $SiO_{2(aq)}$ (n_H). 20

6 Inlet cement equilibrated pore-water solutions derived from NaCl– and $NaHCO_3$–type groundwaters used in the theoretical calculations. 31

7 Mineral name abbreviations and their chemical formulae. 38

List of Figures

1 Solubility of amorphous silica in a NaOH solution plotted as a function of pH. The solid curve is fitted to the data using the tetramer species with a log K of 13.1, and the data in the EQ3/6 data base for the species $H_3SiO_4^-$ and $H_2SiO_4^{2-}$. The dashed curve refers to the monomer species only. At high pH there exists considerable deviation between the dashed curve and the experimental data points indicating that additional silica species, such as the tetramer species, must become important. 6

2 Total concentrations of silica and calcium, and C/S solid ratio in a SiO_2–$Ca(OH)_2$ solution plotted as a function of pH. The curves are calculated using stoichiometric phases of the indicated composition by fitting the equilibrium constants to the experimental points. An extended Debye–Hückel activity coefficient correction is applied to determine the aqueous solution composition. Triangles refer to data from Greenberg and Price (1957), circles and squares to data from Greenberg and Chang (1965). 8

3 Schematic illustration showing the infiltration of groundwater from the surrounding marl host rock through a cement based radioactive waste repository and returning to the marl host rock. 24

4 Propagation of the pH–front into Cretaceous Valanginian marl with time for infiltration of (a) $NaHCO_3$–derived water, and (b) NaCl–derived water. The different curves give the pH profile plotted as a function of the logarithm of distance in meters for times indicated in the figure. Note that an additional front not shown in the figure occurs further downstream, referred to as a salinity wave, where the inlet fluid comes in contact with the original marl groundwater. . . . 37

5 Mineral volume fractions of the primary marl assemblage (a) and secondary minerals (b, c) plotted as a function of the logarithm of the distance from the repository after an elapsed time of 10,000 years for the solid phase evolution resulting from the $NaHCO_3$ inlet solution. Note the different vertical scales for secondary minerals. 39

6 Mineral volume fractions of the primary marl assemblage (a) and secondary minerals (b, c) plotted as a function of the logarithm of the distance from the repository after an elapsed time of 10,000 years for the solid phase evolution resulting from the NaCl inlet solution. Note the different vertical scales for secondary minerals. 40

7 The evolution of porosity for infiltrating (a) $NaHCO_3$– and (b) NaCl–derived groundwaters plotted as a function of the logarithm of the distance at various times indicated in the figure. 41

8 Solution composition for the $NaHCO_3$-derived inlet fluid for a selected set of species: (a) Ca, K, SiO_2–; (b) Na, SiO_2–; and (c) Mg, Al–bearing species plotted as a function of the logarithm of the distance for an elapsed time of 10,000 years. 43

9 Time variation of: (a) pH, and (b) concentrations of species Na^+, K^+ and Ca^{2+}, for the alkali inlet solution assuming a decaying exponential release discussed in the text. 44

10 The evolution of pH and porosity for the alkali-release inlet solution plotted as a function of the logarithm of the distance at various times indicated in the figure. 45

1 INTRODUCTION

A problem of increasing concern is the possible effect of a hyperalkaline plume migrating from a cement-based low and intermediate-level radioactive waste repository on the surrounding host country rock. The country rock forms a geological barrier which can retard the migration of radionuclides to the biosphere. Interaction between groundwater and a concrete-based repository could potentially mobilize a strongly alkaline fluid from the repository. Under such conditions the primary mineral assemblage is likely to be thermodynamically unstable, thus significant alteration of the host rock could result. Changes in porosity and permeability are expected to occur as host rock minerals become unstable and dissolve and are replaced by various secondary mineral assemblages. Ion exchange and adsorption processes may also be affected as a consequence of aqueous complexing reactions with alkali and generation of secondary mineral products. Thus a high pH fluid could have a significant effect upon the performance of the repository, with regard to the ability of the host rock to retard the migration of radionuclides to the biosphere.

Freshly hydrated (set) cement contains a highly alkaline pore water solution with pH-values around 13 (Lea, 1970). Because of the very limited solubility of calcium silicate hydrate and saturation of the pore water with portlandite, degradation of the cement matrix in a underground waste repository proceeds extremely slowly (Berner, 1990; Reardon, 1992). Two questions of fundamental importance that need to be addressed are: (i) to what extent is the pH of the plume neutralized to lower values as a result of mineral reactions with the marl host rock; and, (ii) how will the resulting alteration products which form from reaction of the hyperalkaline plume with the host rock affect the integrity of the repository, i.e. what are the possible changes in porosity, permeability and tortuosity of the host rock?

To address these questions several simplified calculations are presented describing the interaction of cement pore fluid with a marl host rock in time and space. Specifically the calculations depict the migration of a hyperalkaline plume discharging from the repository as it comes in contact with and infiltrates into a marl host rock. A time-space continuum formulation of mass transport in a one-dimensional porous medium employing a kinetic description of mineral reactions is used in the calculations. The transport model takes into account advective transport of solute species assuming local chemical equilibrium of aqueous complexes. Minerals considered in the calculations include dissolution of clay minerals and precipitation of alteration

products including cementitious phases, zeolites and feldspars. Several different cement pore fluid compositions of hyperalkaline waters emerging from the repository are considered. To enable integration of the governing equations over sufficiently long time spans to observe migration of the hyperalkaline plume as described by the model, the quasi-stationary state approximation or multiple reaction path approach is used. The calculations are based on the simplification that changes in porosity and permeability can be neglected during alteration of the marl host rock. The calculations themselves, however, demonstrate that this is a gross over-simplification and that strong alteration of the host rock and consequent changes in porosity, permeability and tortuosity are to be expected. Nevertheless, the results are useful in providing a qualitative representation of the gross features of interaction of cement pore water with a marl host rock. Recently, Steefel and Lichtner (1994) have analyzed the consequeces of diffusion of a hyperalkaline plume into a marl host rock incorporating changes in porosity and tortuosity.

Another purpose of this work is to elucidate the complex geochemistry involved under conditions of high pH. This is a complex subject and many aspects of fluids and their interaction with minerals at hyperalkaline conditions are understood only poorly. The degradation of cement itself is not well-understood especially concerning the release of alkalies which controls the pH of the cement pore fluid during the early stages of degradation. The alteration products which form as a hyperalkaline fluid interacts with marl can only be guessed at this time. Nevertheless, in spite of these uncertainties, it is believed that certain features of the process will remain intact as more details become known and it is hoped that this work will encourage others to pursue these topics through future research. It cannot be emphasized enough, however, that this work does not address the important issues of degradation of the cement and the likelihood that marl groundwater will reach equilibrium with cement in the repository to produce a hyperalkaline plume.

2 GEOCHEMICAL CHARACTERIZATION OF THE CEMENT AND MARL SYSTEMS

2.1 Cement Composition

The Portland cement materials which are currently being considered or are already in use in many countries for construction of low-level radioactive waste disposal sites, have been known for only approximately the last 150 years (Mallison and Davies, 1987; Thomassin and Rassineux, 1992). Since that time intensive research programs have been carried out to study cement hydration (Sarkar et al., 1982; Atkins et al., 1991; Bennett et al., 1992). An overview of the extremely complex thermodynamics of mixed phases in cement has been given by Lea (1970). Unfortunately, hydrated cements contain a series of very complex (in terms of composition) phases which often form solid solutions with varying thermodynamic properties. Furthermore, some of these solids are difficult to identify because of their cryptocrystalline form. The solid phase system becomes even more complex with addition of various additives (e.g. fly-ash, trass) to the cement material. However, a simplified solid phase composition based on hydration model concepts (Berner, 1987; Glasser et al., 1988; Reardon, 1992) is compatible with analytical pore water data (Kalousek, 1952; Greenberg and Chang, 1965; Greenberg and Price, 1957; Atkinson et al., 1987).

Predicting the evolution of solid and pore water chemistry of cement-water systems with time is an extremely complicated endeavor and an active area of research (see Reardon (1992) for a lucid account). The original anhydrous material and hydrated alteration products are highly reactive in water, their rates of reaction most probably limited by diffusive transport within the cement pore spaces. Alteration products form protective armored coatings on mineral surfaces limiting the rate of diffusion to the reactive cores and thereby preventing a static thermodynamic equilibrium state of the cement-water system from being achieved. As a consequence the cement chemistry evolves continuously over time.

Especially important to the short-term evolution of the pH of the cement pore solution is the release of alkalies from the solid phases. Alkalies are contained in readily-soluble sulfates and as minor constituents in clinker phases with potassium-rich solids in greater abundance than sodium-rich as a result of the kiln firing process. In the absence of alkalies, the cement

pore solution can be represented as an invariant mineral assemblage with a pH of approximately 12.5 (Reardon, 1992). However, as alkalies are slowly added to solution by diffusive transport through altered layers surrounding the reactive cores, the pH rises dramatically in order to maintain electroneutrality of the solution. At present there is no proven theoretical method for predicting the concentration of alkalies in a cement pore fluid given the solid phase abundances and empirical estimates must be used (Reardon, 1992).

Two phases generated during cement hydration can be extremely important for determining the cement pore solution chemistry. These are $Ca(OH)_{2(s)}$ (portlandite) and C_xSH_y (calcium silicate hydrate, CSH). The latter forms one or more solid solutions by reaction of water with the anhydrous cement phases C_3S and C_2S (notation from the cement literature is used: C = CaO, A = Al_2O_3, S = SiO_2, F = Fe_2O_3, H = H_2O), indicated schematically by the reactions:

$$(CaO)_3 \cdot SiO_2 + (3 - x + y)\, H_2O \rightarrow (CaO)_x \cdot SiO_2 \cdot yH_2O + (3 - x)\, Ca(OH)_{2(s)}, \quad (1)$$

and

$$(CaO)_2 \cdot SiO_2 + (2 - x + y)\, H_2O \rightarrow (CaO)_x \cdot SiO_2 \cdot yH_2O + (2 - x)\, Ca(OH)_{2(s)}. \quad (2)$$

Portlandite also forms from hydration of free lime according to the reaction

$$CaO + H_2O \rightarrow Ca(OH)_{2(s)}. \quad (3)$$

This reaction is usually of lesser importance due to the small (less than 1%) quantities of free lime in typical cement. However, the cement envisaged in construction of the Swiss repository, known as Sulfacem, may contain as much as 10% free lime. The composition of Sulfacem is given in Table 1.

The relatively high solubility of portlandite, and limited solubility of the CSH-phases and residual alkalies, lead to a high hydroxide but relatively low silica activity of the cement pore solution. The low activity of silica ($\sim 10^{-5}$ M) and high pH in cement pore solutions leads to aggressive alteration of the host rock forming the geologic barrier to radionuclide transport. The dissolution of clay minerals and consequent formation of secondary phases depend strongly on the activity of silica in solution. Because of the large volume change of reaction associated with precipitation of calcium silicate and aluminate hydrate minerals (CSH– and CAH–phases) compared to typical rock-forming minerals, rapid filling of the available pore space can result and hence reduction in the permeability of the porous medium. The presence

of CSH-gels and other cement-type minerals, including hydrogarnet and zeolites, have been observed in rock/water interaction experiments (Johnston and Miller, 1984a, b; Savage et al., 1990, 1991). The formation of secondary amorphous and cryptocrystalline CSH-phases such as okenite, foshagite, tobermorite and hillebrandite, in addition to zeolites and authigenic feldspars (probably derived from dissolution of clay minerals), have been observed in a natural analogue of a cementitious system in northern Jordan (Khoury and Nassir, 1982; Milodowski, et al., 1992).

Table 1: Composition of Sulfacem weight percent dry material (taken from Berner, 1990, Table 4).

Oxide	wt. %	Clinker Composition	wt. %
CaO	62–63	C_3S	45–50
SiO_2	20–21	C_2S	20–22
Al_2O_3	2.8–4.2	C_3A	0
Fe_2O_3	7.0–7.5	C_4AF	18–20
SO_3	2.5–3.0	C_2F	0–2
K_2O	1.0†		
Na_2O	0.1†		
MgO	1.0†		
$CaCO_3$	—		

† Assumed value.

Because of the high pH associated with the cement pore solution, large quantities of SiO_2 would dissolve if silica solubility limiting solids did not form (cf. Eikenberg, 1990). Because of the formation of CSH-gels with extremely low solubilities in the SiO_2–CaO–H_2O–system, silica concentration is limited to very low values. The large difference in silica solubility in sodium- and calcium-hydroxide solutions can be seen in Figs. 1 and 2. In Fig. 1 the experimentally determined total concentration of dissolved silica for a NaOH solution in equilibrium with amorphous silica is plotted as a function of pH along with two theoretical curves. A best fit to the experimental data is obtained by including the tetramer species $H_6Si_4O_{12}^{2-}$ in addition to monomeric silicic species H_4SiO_4, $H_3SiO_4^-$ and $H_2SiO_4^{2-}$ depicted by the solid line. The dashed line refers to the predicted solubility if only monomer species are included. A log K = 13.1 for

formation of the tetramer species corresponding to the reaction

$$4\,SiO_{2(aq)} + 4\,H_2O \rightleftharpoons H_6Si_4O_{12}^{2-} + 2\,H^+, \qquad (4)$$

is used which compares well with the value of 12.88 given by Busey and Mesmer (1977). However, the existence of this species is still uncertain experimentally. As is apparent from the figure, at pH values exceeding 11, additional low molecular silica polymers such as tetramers can contribute significantly to the aqueous speciation of silicic acid (Busey and Mesmer, 1977; Thornton and Radke, 1988; Eikenberg, 1990).

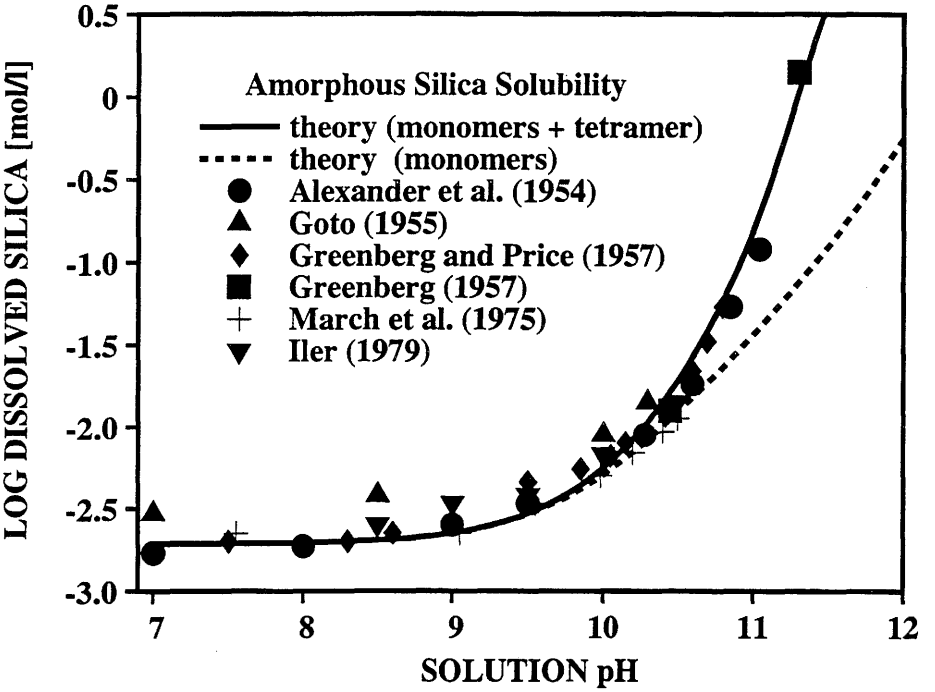

Figure 1: Solubility of amorphous silica in a NaOH solution plotted as a function of pH. The solid curve is fitted to the data using the tetramer species with a log K of 13.1, and the data in the EQ3/6 data base for the species $H_3SiO_4^-$ and $H_2SiO_4^{2-}$. The dashed curve refers to the monomer species only. At high pH there exists considerable deviation between the dashed curve and the experimental data points indicating that additional silica species, such as the tetramer species, must become important.

An entirely different behavior of dissolved silica with increasing pH occurs in the system $CaO–SiO_2–H_2O$ as shown in Figure 2. Greenberg and Chang (1965) measured total silica

and calcium concentrations as well as the Ca–Si molar ratio (C/S) of solids in equilibrium with a calcium hydroxide solution as a function of pH. To understand this result in simple terms, without resorting to one or more solid solution representations of CSH-gels, a series of stoichiometric phases is considered. This approach, if successful, has the advantage of being directly applicable to the time-space transport model which in its present form does not provide for incorporating solid solutions. In Fig. 2 the experimental results together with a theoretical fit to the data based on equilibrium with stoichiometric CSH-phases okenite, tobermorite, foshagite, and hillebrandite are shown. The equilibrium constants of these phases were adjusted slightly (within 5–10%) from the values given in the EQ3/6 data base (Wolery, 1992, adapted from Sarkar et al., 1982) to obtain a reasonable fit to the experimental points (see Table 2). The original values for the equilibrium constants gave results with considerably lower silica and calcium concentrations compared to the experimental data. Because the experiments undoubtedly involved amorphous rather than crystalline phases, it should not be expected to obtain a good fit to the more stable crystalline phases as represented by the thermodynamic data base which should yield lower concentrations of silica and calcium. Ultimately the correct explanation for the data must involve one or more solid solutions representing CSH-gels. Nevertheless, it is useful to understand qualitatively the behavior of dissolved silica in this system in terms of simple stoichiometric phases.

Table 2: Comparison of equilibrium constants for CSH-type phases fitted to experimental solubility data and taken from the EQ3/6 data base.

	log K	
mineral	fitted value	EQ3/6 data base
okenite	11.25	10.38
tobermorite	69.00	63.84
foshagite	63.00	65.92
hillebrandite	36.30	36.82

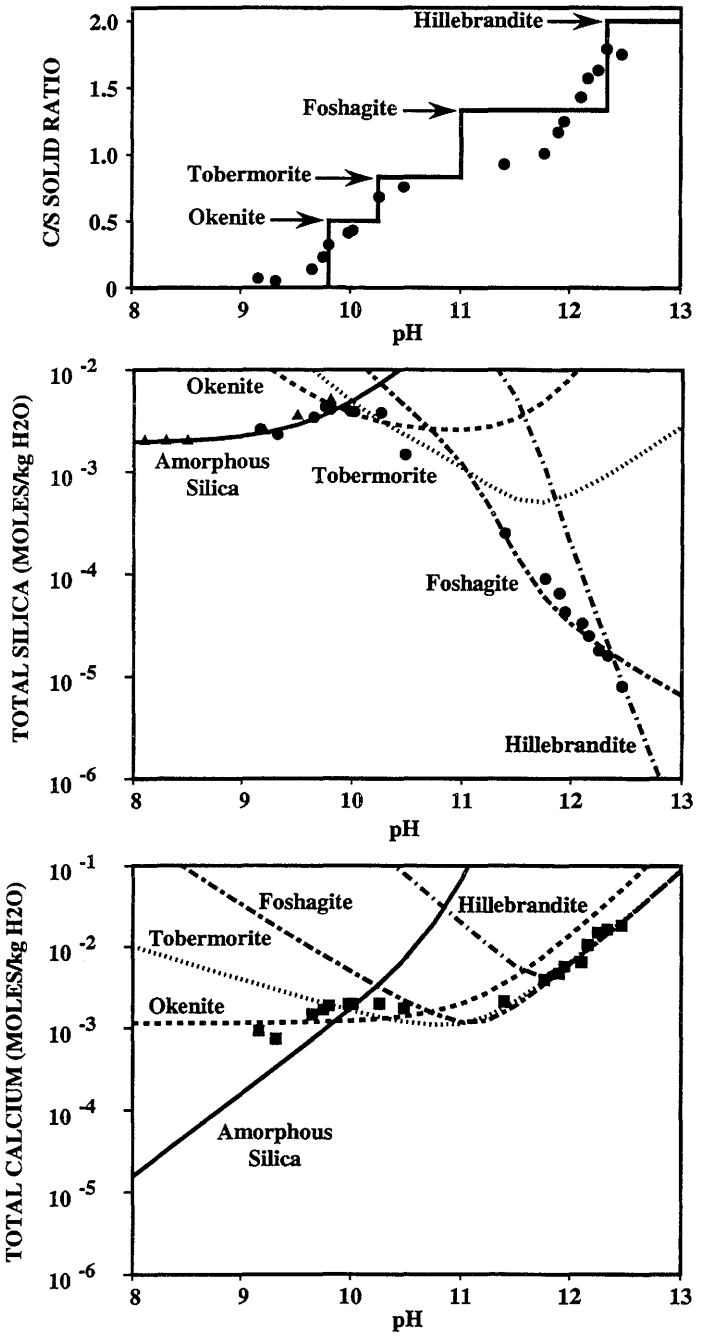

Figure 2: Total concentrations of silica and calcium, and C/S solid ratio in a SiO_2–$Ca(OH)_2$ solution plotted as a function of pH. The curves are calculated using stoichiometric phases of the indicated composition by fitting the equilibrium constants to the experimental points. An extended Debye–Hückel activity coefficient correction is applied to determine the aqueous solution composition. Triangles refer to data from Greenberg and Price (1957), circles and squares to data from Greenberg and Chang (1965).

As these figures demonstrate, the $SiO_{2(s)}$ solubility in both systems is almost identical up to pH 10. However, in more concentrated $Ca(OH)_2$ solutions, CSH-gels form. Due to the limited solubility of these phases, the silica activity in solution actually decreases with increasing pH in the $CaO–SiO_2–H_2O$-system. In contrast, in a pure sodium hydroxide solution, the SiO_2 solubility increases with increasing pH, due to deprotonation and polymerization reactions. Although in the $CaO–SiO_2–H_2O$-system there exists a continuous distribution of CSH–phases with a continuously varying C/S–ratio, it is remarkable that representation by crystalline phases results in a step-wise behavior of the C/S ratio which reasonably approximates the relatively smooth variation obtained experimentally. The fit to the total calcium concentration is not as good at low pH compared to high pH. At high pH the theoretical curve is determined by charge balance between Ca^{2+} and OH^-, whereas at low pH the curve is determined by charge balance with Ca^{2+} and the species $H_3SiO_4^-$.

2.2 Marl Composition

Wellenberg has been chosen as the preferred location for the disposal of low and short-lived intermediate level radioactive wastes in Switzerland. Here, target geological formations comprise the Cretaceous Palfris formation and Vitznau Marls, formerly known in a generic sense as the "Valanginian Marl." These rock sequences are strongly folded and build up tectonically complex structures. The mineralogical composition of the marl can be described as an aggregate of aluminosilicates (mainly in the form of clay minerals and chlorites), calcite and quartz. In contrast to the relatively homogeneous chemical composition of the cement mass in the repository, the marl has large percentage differences in the volumes of the mineral components. For example, the fraction of aluminosilicates may exceed 40 vol%, but with significantly less calcite (30 vol%). As the calcite component increases, the aluminosilicate fraction decreases, reaching approximately 15 vol% in extreme cases. An average modal mineralogical composition of the marl host rock used in the calculations is given in the first column of Table 3. Also given in the table is the composition of a reference fault gouge and shaly marl. These differ primarily in the amount of calcite and clay minerals. Also the shaly marl contains twice as much dolomite. The added amounts of clay minerals should increase the potential for neutralizing the high pH pore waters emanating from the cement matrix.

Table 3: Modal composition [vol %] of the marl rock type considered in this study.

Mineral	This study	Fault gouge†	Shaly marl†
calcite	42	13.5	26.5
dolomite	5	4.5	9
quartz	15	13.5	18
pyrite	1	1.5	1.5
illite, illite–smectites	20	44	32
chlorite	7	13	11
porosity	10	10	2

† Reference composition derived from NTB 93-28, Fig. 4.3.3.

The chemical composition of two typical Wellenberg groundwaters are given in Table 4. The first corresponds to a relatively strongly mineralized NaCl-type water ($I \sim 0.1$ M), and the second to a more weakly mineralized $NaHCO_3$-type water ($I \sim 0.02$ M). While the former type is characterized by $\delta^{18}O$–δD isotope data which can probably be related to a very old (Cretaceous) fossil sea water, the younger bicarbonate water has an isotopic composition similar to that of meteoric precipitation. Nevertheless, due to the lack of nuclear-detonation derived tritium, the latter water is at least 30–50 years in age. The older NaCl water is found predominantly within the relatively dense rock matrix, while the younger $NaHCO_3$ water percolates preferentially through regions of higher hydraulic conductivity including fracture zones (NAGRA, unpublished data). The possibility of interaction of both waters with the cementitious barrier of the near-field can lead to different cement pore water compositions, and hence both types are considered in the modeling study presented below.

Table 4: Chemical composition of two marl groundwater types from the Wellenberg region [mol l^{-1}].

	NaCl–type this study	NaCl–reference water (NTB 93-28, Table 5.1.6)	$NaHCO_3$-type this study	$NaHCO_3$-reference water (NTB 93-28, Table 5.1.5)
Na^+	1.78×10^{-1}	4.61×10^{-1}	1.83×10^{-2}	1.76×10^{-2}
K^+	3.32×10^{-4}	7.10×10^{-4}	1.02×10^{-4}	5.11×10^{-5}
Ca^{2+}	4.11×10^{-3}	4.50×10^{-3}	1.20×10^{-4}	5.74×10^{-5}
Mg^{2+}	2.45×10^{-4}	3.38×10^{-3}	8.35×10^{-6}	3.29×10^{-5}
Sr^{2+}	3.11×10^{-5}	7.04×10^{-4}	9.12×10^{-7}	5.71×10^{-6}
$C_{(tot)}{}^a$	2.10×10^{-3}	4.01×10^{-3}	1.35×10^{-2}	1.64×10^{-2}
$Si_{(tot)}{}^b$	1.02×10^{-4}	2.06×10^{-4}	1.91×10^{-4}	1.74×10^{-4}
SO_4^{2-}	5.70×10^{-4}	1.07×10^{-5}	1.43×10^{-3}	1.15×10^{-4}
F^-	3.51×10^{-4}	9.20×10^{-7}	1.39×10^{-3}	9.47×10^{-4}
Cl^-	1.84×10^{-1}	4.73×10^{-1}	1.03×10^{-3}	2.82×10^{-4}
T[°C]	25	25	25	25
I[M]	0.2	0.49	0.02	0.0181
pH	7.6	7.5	8.0	8.3
log pCO_2[bar]	−2.7	−2.3	−2.1	−2.31
approximate saturated minerals	calcite dolomite strontianite fluorite quartz	calcite dolomite strontianite chalcedony rhodochrosite	calcite dolomite strontianite fluorite chalcedony	calcite dolomite strontianite chalcedony rhodochrosite siderite

$^a C_{(tot)} = H_2CO_3 + HCO_3^- + CO_3^{2-}$

$^b Si_{(tot)} = SiO_{2(aq)} + H_3SiO_4^- + H_2SiO_4^{2-}$

3 INTERACTION OF ROCK WITH HYPERALKALINE FLUIDS

This chapter focuses on water–rock interaction processes of rock–fluid systems that have been infiltrated by cement pore fluids. Likely mineral and cation exchange reactions are discussed and compared with results from alkaline flooding and alkali titration experiments as well as with observations of natural systems. It should be noted that these processes need not necessarily reflect those processes which take place in the repository environment. This is because of (i) the relatively short duration of the rock-water interaction experiments in the laboratory (weeks to months) compared to the much longer travel times of the repository inventory through the geosphere (hundreds of thousands of years) and (ii) differences in modal rock composition and composition of the infiltrating solution.

3.1 Alkaline Flooding

Rock types usually encountered in alkaline flooding are sandstones containing only minor amounts of clay minerals and carbonates. It is, however, known that the pore water chemistry of hydrated concrete which includes large amounts of quartz gravel is very similar to the pore solution of a pure hardened cement paste (Lea, 1970). Therefore, because of the absence of clay minerals and the short time spans of alkaline solution injection, the pH neutralization effect of quartz rich sediments flooded by alkaline solutions is certainly less significant compared to a system where primary clay minerals dissolve to form a stable secondary mineral paragenesis.

Nevertheless, because long term rock-water interaction experiments using Valanginian marl and cement solutions have not yet been performed under moderate repository PT-conditions, the literature data are helpful to identify qualitatively the relevant chemical processes which should be considered in this study.

Considerable attention over the past twenty years has been devoted towards understanding the processes involved in alkaline flooding techniques applied to enhanced oil recovery. Successful engineering application rests on the ability of hyperalkaline fluid to penetrate rapidly large portions of an oil reservoir where hydrocarbons are typically trapped in steeply dipping porous sandstone layers discordantly overlain by non-transmissive formations. The alkaline solution neutralizes organic acids contained in oil, allowing the oil to become mobilized (deZabala

et al., 1982). For the flooding technique to be successful, the pH must be maintained above a minimum threshold level (Cooke et al., 1974). The degree to which the pH is neutralized and the extent of penetration of the hyperalkaline plume is dependent on the interaction of the injected alkaline fluid with the reservoir host rock. Early studies noted that reaction between hyperalkaline solutions and reservoir rocks produced only relatively small drops in pH and concluded that caustic loss by rock reaction should not be severe (Mungan, 1979, Jennings et al., 1974; Sydansk, 1982). However, subsequent laboratory and field recovery tests have not been as encouraging as a result of pH loss and retardation of the alkaline pulse (Jensen and Radke, 1988).

Because of the short time scales involved, the processes which result in hydroxide consumption during alkaline flooding are primarily ion-exchange reactions, and, probably to a much lesser extent congruent and incongruent mineral precipitation and dissolution. Most modeling efforts have involved ion-exchange reactions (Bunge and Radke, 1982, 1983, 1985). These authors consider exchange reactions between sodium, calcium and the hydronium ion of the form

$$\bar{M}H + Na^+ \rightleftharpoons \bar{M}Na + H^+, \tag{5}$$

and

$$2\bar{M}H + Ca^{2+} \rightleftharpoons \bar{M}_2Ca + 2H^+. \tag{6}$$

The symbol $\bar{M}$ denotes a negatively charged mineral surface site. The importance of ion-exchange reactions on pH during alkaline flooding was demonstrated experimentally by Novosad and Novosad (1984).

In a more recent model study, Bryant et al., (1986) considered mineral precipitation and dissolution reactions as well as ion-exchange reactions for local equilibrium conditions. They compared their model calculations with experimental results of Bunge et al., (1980) and Bunge and Radke (1982) for injection of high pH brine into Wilmington sandstone and obtained good agreement with the experimental results. Very little pH loss was reported from the experiment and the theoretical calculations gave conservative results indicating a slightly greater pH drop. Bunge and Radke (1985) also performed flow-through laboratory experiments and obtained good agreement with calculations based on a lumped parameter model. SEM analysis of the cores showed the presence of zeolites, possibly phillipsite.

For injection of alkaline solutions to be a promising method for improving oil recovery, the

rate of chemical interaction between the injected alkaline solution and the sandstone reservoir is of great importance. The kinetics of quartz dissolution and precipitation as a function of pH was investigated experimentally by Thornton and Radke (1988), and Schwarzentruber et al. (1987) at elevated temperatures of 90°C. It was generally observed that the dissolution rate of quartz strongly increases with pH via "first-order" kinetics and this effect was interpreted by a pH-dependent adsorption of silica layers on the quartz surface. The solubility of silica at high pH has been investigated recently in a combined model and literature study and thermodynamic equilibrium constants were recommended for 3 monomeric and 6 polymeric silica species (Eikenberg, 1990). However, much more work needs to be done before a reliable thermodynamic data base is available and a complete understanding of the processes involved is obtained.

3.2 Alkali and Calcium Hydroxide Titration Experiments

Alkaline titration experiments using clay rich sediments, mineralogically comparable to Valanginian marl, were performed by Johnston and Miller (1984a, b), Ewart et al. (1985) and Jefferies et al. (1988). Titration of a $Ca(OH)_2$ solution on Oxford Clay caused pH neutralization over the entire range of the experiment, 1–20 meq $Ca(OH)_2$ per 100g clay (Ewart et al. 1985). A marked decrease in the Mg^{2+} and aluminum concentrations with increasing titrated $Ca(OH)_2$ concentration was measured. It was concluded that Ca^{2+} was replaced by other, primarily polyvalent, cations adsorbed on clay minerals. As a consequence, Mg- and Al-hydroxides (such as brucite) exceeded their solubility limits and precipitated. A simplified exchange reaction of this type causing pH neutralization can be formulated as follows:

$$\text{Mg} - \text{montmorillonite} + \text{Ca}^{2+} + 2\,\text{OH}^- \rightleftharpoons \text{Ca} - \text{montmorillonite} + \text{Mg(OH)}_2 \downarrow . \quad (7)$$

In a comparable experiment on London Clay using pure NaOH solutions instead of $Ca(OH)_2$, a similar pH neutralization was observed up to pH 10 (10^{-2} M NaOH). Since the exchange sites of the clay minerals of this sediment were initially covered with Mg^{2+}–ions it was again proposed that cation exchange reactions lead to brucite precipitation which caused the observed pH neutralization. Additional model calculations using the geochemical code PHREEQE including cation exchange reactions proved to be consistent with this conclusion. However, above pH 10 no further neutralization occurred. This indicated that beyond the threshold value of pH 10 (for a system of 1g clay in 18 ml solution) all Mg^{2+} was exchanged from the surface sites and that within the time of the experiments (3-4 days) negligible dissolution of clay minerals could

have taken place. Based on these experimental observations a modeling study by Haworth et al. (1987) using the transport code CHEQMATE came to the conclusion that the propagation of high pH waters from a repository into a clay formation is slightly retarded due solely to cation exchange reactions.

In alkali and $Ca(OH)_2$ titration experiments on a calcium bentonite which lasted for a longer time period of 30 days, Johnston and Miller (1984a, b) observed dissolution of bentonite in concentrated $Ca(OH)_2$ solutions at 25°C and confirmed formation of zeolite phases using X-ray diffraction analysis. These phases were very similar in structure to the zeolite mineral phillipsite. In titration experiments using KOH solutions (at 150–250°C), an analcime-type zeolite and potassium feldspar were determined as secondary phases.

More recently, experiments conducted by Chermak at the Universität Bern studied the effect of high pH solutions on Swiss Opalinus shale at 175°C in closed system batch experiments. The disappearance of kaolinite, chlorite and fine grained quartz was observed with formation of analcime, smectite and interlayered mica smectite (with 0.1 M NaOH solution); and potassium feldspar, phillipsite and interlayered mica/smectite (with 0.1 M KOH solution). Geochemical model calculations were consistent with the measured evolution of the pH as a function of time (Chermak and Lichtner, 1991).

3.3 Natural Analogues

In addition to experimental studies, natural analogue systems provide data on the interaction of hyperalkaline cement pore waters with sedimentary systems. One of the main advantages of natural analogue systems is that natural processes usually involve a much longer time span compared to experimental investigations and hence are more realistic for long term predictions of radwaste scenarios. Unfortunately, as noted above, portland-type cements have been produced only in the last $\approx$ 150 years. Older cement buildings, some as old as 8000 years, do not contain the typical mineral assemblages found in modern portland cements (Mallison and Davies, 1987). In addition, since the groundwater around most man-made cement constructions typically invades the cement materials, but not the reverse (i.e. flow from the cement into the geosphere), most cement constructions are not suitable as natural analogue systems for the problem considered in this study. Furthermore, for cement constructions located close to the

surface, the pH–neutralization of hyperalkaline cement pore waters is not due entirely to clay mineral dissolution, but may result from reaction with dissolved CO_2 from the atmosphere. Clearly, carbonic acid may also strongly dissolve the mineral portlandite in the cement matrix. A detailed mineralogical description of calcification of portlandite at the contact zone between cement and marl in samples from the "Seelisberg" tunnel (Valanginian marl) has been given by Mazurek (1991). He concluded that infiltration of a bicarbonate fluid caused the alteration of cement in this zone, according to a reaction of the form:

$$HCO_3^- + H^+ + Ca(OH)_{2(s)} \rightarrow CaCO_{3(s)} + 2\,H_2O, \qquad (8)$$

in which calcite is produced through consumption of bicarbonate and hydrogen ions present in the marl groundwater as it reacts with portlandite.

Despite these problems, an interesting natural analogue system was found located in Northern Jordan (Khoury et al., 1985; Khoury and Nassir, 1982). Here bituminous calcareous limestones are percolated by hyperalkaline groundwaters which are saturated portlandite solutions with pH values around 12.5 (Khoury et al., 1985). These unusually high pH values can be explained as a result of spontaneous combustion of organic material providing heat for decarbonization reactions (formation of lime). Subsequent reaction with water led to formation of a complex sequence of secondary cement type minerals such as portlandite and CSH-phases. Therefore, this site provides an ideal example of a natural analogue of a cementitious waste repository. An overview of the current status of investigations at this site has been given recently by Alexander (1992). Currently, investigations are underway to determine if, at specific locations, high pH waters infiltrated directly into uncombusted sedimentary formations consisting of clay minerals, calcite, quartz and organic materials. The results from such a study area could be of great importance to determine likely secondary mineral products for use in geochemical codes for predicting the propagation of a high pH–front. Perhaps most important are indications from preliminary field investigations (Milodowski et al., 1992) which document the formation of isolated pathways sealing the rock matrix from the fracture network. This creates preferential paths for transport of radionuclides which are not able to react with the host rock and are transported directly to the biosphere without retardation. These observations are in agreement with numerical calculations discussed below and could lead to a deleterious scenario for transfer of radionuclides from a cementitious repository.

3.4 Importance of Cation Exchange and Clay Dissolution Reactions

In general, comparison of modeling results based on ion-exchange reactions with laboratory titration experiments and alkaline flooding studies yielded good agreement, both for the depletion in pH of the hyperalkaline plume and its rate of advance in flow experiments. This is not surprising because short term exposure of clay minerals to alkaline solutions causes cation exchange reactions to proceed extremely rapidly (within days), whereas clay dissolution and subsequent precipitation of alteration products, is generally a very slow process at moderate PT-conditions (Johnston and Miller, 1984b). Such systems may evolve over decades of years. It should also be noted that the exchange of cations Na^+ and K^+ with Ca^{2+} in a $Ca(OH)_2$ medium has a stabilizing effect on the montmorillonite/illite layers (cf. Grauer, 1988). Further alteration of these phases may thus be kinetically inhibited.

It must be realized that processes important for the technical realization of alkaline flooding, may be minor when viewed on geologic time scales. For example, for injection and recovery wells separated by a distance of 100m (typical in engineering practice), and assuming an average fluid flow rate of 1 km y^{-1}, it would take approximately 1 month for a non- reacting species to traverse the distance between the wells. For a reacting species with a retardation factor of 10 it would take one year. A time delay for the alkaline pulse of this magnitude is not economically feasible and therefore long term data are not available from the alkaline flooding literature. In a nuclear waste repository which includes cemented waste blocks and reinforced concrete there is, however, sufficient alkali and calcium hydroxide present to produce a hyperalkaline plume for tens of thousands of years.

Therefore, it is likely that clay minerals in the host rock surrounding a cement based repository dissolve continuously to produce various secondary mineral assemblages. Compared to surface cation exchange reactions, clay dissolution in a high pH fluid has a much stronger pH neutralization effect. Consider, for instance, an illite/smectite layer with a high cation exchange capacity of 25 meq/kg and assume that the exchange sites are completely covered by bivalent ions. Taking a Ca^{2+}/Mg^{2+} ratio of $\sim$ 2, typical of Valanginian marl groundwater (see Table 4), and similar sorption competition between these cations (i.e. ${}^{Mg}_{Ca}K_c \sim 1$), it follows that the fractional occupancy of Mg^{2+} is 30% of the total cation exchange capacity, i.e. $\sim$ 8 meq/kg. If all Mg^{2+} is replaced by Ca^{2+} due to infiltration of portlandite saturated solutions, and all Mg^{2+} is precipitated as brucite, then 16 meq or $\sim$ 270 mg hydroxide would be involved in reaction

with 1 kg clay minerals. If, however, the same clay minerals were to react with $Ca(OH)_2$ in a 1:1 stoichiometric ratio to form zeolites, then dissolution of 1 kg clay with a molecular mass of $\sim$ 400 g/mole would neutralize $\sim$ 2.5 eq or $\sim$ 40g hydroxide, i.e. this process involves approximately 150 times more OH^- compared to cation exchange reactions.

4 PHASE EQUILIBRIA AND pH–CONTROLS

To study the reactions between a high pH alkaline plume and host rock minerals, the speciation of the aqueous solution at high pH conditions has to be taken into account. Typically, rock forming minerals in Valanginian marl are calcite, quartz, illite/smectite, and chlorite. The dissolution of the latter minerals are strongly pH dependent because of hydrolysis and/or dissociation reactions of alumina and silica species.

Reactions with silicate minerals at high pH tend to produce protons thereby reducing the pH. This is just the opposite of behavior at low pH in which protons are consumed by hydrolysis reactions thereby increasing the pH. The qualitative effect of aluminosilicate mineral hydrolysis reactions on pH can be investigated by comparing reactions written in terms of species $Al(OH)_4^-$ and $H_3SiO_4^-$ with those written in terms of the species Al^{3+} and $SiO_{2(aq)}$. Although this is a rough simplification, for it assumes that other complexes with cations such as Ca^{2+}, Mg^+ or Na^+ are negligible (which is not always the case at high pH), it shows qualitatively the effect of pH in terms of stoichiometric coefficients.

The general hydrolysis reaction of an aluminosilicate mineral $\mathcal{M}$ can be written in the form

$$\mathcal{M} \rightleftharpoons \mathcal{P} + n_{Al}\,Al^{3+} + n_{Si}\,SiO_{2(aq)} + n_H\,H^+ + n_{H_2O}\,H_2O. \tag{9}$$

for product species $\mathcal{P}$ other than Al^{3+}, $SiO_{2(aq)}$, H^+ and H_2O, where the coefficients n_{Al} and n_H denote the stoichiometric coefficients of Al^{3+} and H^+, respectively. In the pH regime above 10 and below 13 (characteristic pH regime of the pore solution evolving during cement degradation) this reaction becomes in terms of the species $Al(OH)_4^-$ and $H_3SiO_4^-$

$$\mathcal{M} \rightleftharpoons \mathcal{P} + n_{Al}\,Al(OH)_4^- + n_{Si}\,H_3SiO_4^- + n'_H\,H^+ + n'_{H_2O}\,H_2O, \tag{10}$$

with

$$n'_H = n_H + 4n_{Al} + n_{Si}, \tag{11}$$

and

$$n'_{H_2O} = n_{H_2O} - 4n_{Al} - 2n_{Si}. \tag{12}$$

For $n_H < 0$, a change in sign of the stoichiometric coefficient for H^+ occurs if

$$4n_{Al} + n_{Si} > -n_H. \tag{13}$$

For example, clinochlore-14A has $n_H = -16$, $n_{Al} = 2$ and $n_{Si} = 3$. This results in $n'_H = 5$. A list of the stoichiometric coefficients for a number of minerals including zeolites and CSH-phases is presented in Table 5. Several examples are presented below in more detail.

Table 5: Stoichiometric coefficients for H^+ for mineral reactions written in terms of the species $Al(OH)_4^-$ and $H_3SiO_4^-$ (n'_H), and Al^{3+} and $SiO_{2(aq)}$ (n_H).

mineral	n'_H	n_H	mineral	n'_H	n_H
silicates					
clinochlore-14A	5	−16	muscovite	5	−10
daphnite-14A	1	−16	quartz	1	0
kaolinite	4	−6	ripidolite-14A	1	−10
zeolites					
analcime	2	−4	heulandite-Ca	7	−8
ashcroftite	5	−16	laumontite	4	−8
brewsterite-Ca	6	−8	levyne	4	−8
chabazite	4	−8	mordenite-Na	5	−12
dachiardite-Ca	19	−20	natrolite	3	−8
epistilbite	6	−8	phillipsite-Ca	5	−12
erionite-Ca	27	−36	scolecite	3	−8
faujasite-Ca	4	−8	stilbite-Ca	7	−8
garronite	10	−24	wairakite	4	−8
gismondine	2	−8	yugawaralite	5	−8
gmelinite-Ca	4	−8			
CSH–phases†					
tobermorite	2	−10	foshagite	−2	−8
hillebrandite	−2	−4			
other cement phases					
katoite	−4	−12	sepiolite‡	2	−8
ettringite	−4	−12	brucite‡	−2	−1

†with species CaH_2SiO_4 ‡with species $CaOH^+$

Calcite: Above a pH of approximately 12.85 the species $CaOH^+$ is the dominant aqueous

calcium species, and dissolution of calcite leads to the reaction

$$CaCO_{3(s)} + H_2O \rightarrow CaOH^+ + H^+ + CO_3^{2-}, \quad (14)$$

resulting in a reduction in pH. If Ca^{2+} is the dominant species then at high pH the dissolution reaction is simply

$$CaCO_{3(s)} \rightarrow Ca^{2+} + CO_3^{2-}, \quad (15)$$

and there is no pH change. In slightly alkaline solutions calcite dissolution is proton consuming according to the reaction

$$CaCO_{3(s)} + H^+ \rightarrow Ca^{2+} + HCO_3^-. \quad (16)$$

Below pH 7 proton consumption is even more effective as demonstrated by the reaction

$$CaCO_{3(s)} + 2\,H^+ \rightarrow Ca^{2+} + H_2CO_3. \quad (17)$$

Thus the dissolution of calcite at low pH increases the pH, and at high pH the pH remains the same or decreases slightly. Clearly the dissolution of calcite is also dependent on the partial pressure of CO_2.

Quartz: The dissolution of quartz for conditions of low pH does not alter the pH of the solution according to the reaction

$$SiO_{2(s)} + 2\,H_2O \rightarrow H_4SiO_4. \quad (18)$$

At high pH, however, assuming $H_3SiO_4^-$ as the dominant aqueous silica species, this reaction can be expressed in the form

$$SiO_{2(s)} + 2\,H_2O \rightarrow H_3SiO_4^- + H^+, \quad (19)$$

resulting in a decrease in pH as quartz dissolves. In the presence of CSH-gels with CaH_2SiO_4 as the dominant aqueous silica species, the following reaction can be expected to take place:

$$SiO_{2(s)} + Ca^{2+} + 2\,H_2O \rightarrow CaH_2SiO_4 + 2\,H^+, \quad (20)$$

resulting in a more effective reduction in pH.

Kaolinite: The hydrolysis reaction for kaolinite at low pH may be expressed as

$$Al_2Si_2O_5(OH)_4 + 6\,H^+ \rightleftharpoons 2\,Al^{3+} + 2\,SiO_{2(aq)} + 5\,H_2O. \quad (21)$$

According to this form of the reaction the pH increases as kaolinite dissolves in acidic solutions. At high pH, assuming the dominant aluminum and silica species are $Al(OH)_4^-$ and $H_3SiO_4^-$, this reaction becomes

$$Al_2Si_2O_5(OH)_4 + 7\,H_2O \rightleftharpoons 2\,Al(OH)_4^- + 4\,H^+ + 2\,H_3SiO_4^-. \qquad (22)$$

In this case the opposite behavior is obtained and the pH decreases as kaolinite dissolves.

Muscovite: The stoichiometrically complex clay minerals illite and illite–smectite are here simplified as muscovite. The hydrolysis reaction of muscovite at low pH can be written as follows

$$KAl_3Si_3O_{10}(OH)_2 + 10\,H^+ \rightarrow K^+ + 3\,Al^{3+} + 3\,SiO_{2(aq)} + 6\,H_2O. \qquad (23)$$

At high pH with $Al(OH)_4^-$ and H_3SiO_4 as the dominant species in solution this reaction becomes

$$KAl_3Si_3O_{10}(OH)_2 + 12\,H_2O \rightarrow K^+ + 3\,Al(OH)_4^- + 3\,H_3SiO_4^- + 5\,H^+. \qquad (24)$$

Thus the dissolution of muscovite at high pH reduces the pH whereas at low pH the pH increases (amphoteric behavior of alumina).

Fe, Mg-chlorite: Chlorites are chemically rather complex. The charge balance resulting from the Si–Al substitution in the tetrahedral sheets is compensated mainly by Fe^{2+}, Mg^{2+} and Al^{3+} in the octahedral interlayers. For simplification of the hydrolysis reactions Mg-chlorite (clinochlore) is given as an example. At low pH the reaction is

$$Mg_5Al_2Si_3O_{10}(OH)_8 + 16\,H^+ \rightarrow 5\,Mg^{2+} + 2\,Al^{3+} + 3\,SiO_{2(aq)} + 12\,H_2O, \qquad (25)$$

while at high pH the hydrolysis reaction can be expressed as

$$Mg_5Al_2Si_3O_{10}(OH)_8 + 7\,H_2O \rightarrow 5\,MgOH^+ + 2\,Al(OH)_4^- + 3\,H_3SiO_4^-, \qquad (26)$$

with $MgOH^+$ as the dominant magnesium species, and thus the pH remains unchanged. In contrast to the other aluminosilicate minerals presented above, the dissolution of chlorites is not as effective in neutralizing alkaline solutions. For this mineral group the pH-neutralization effect becomes more efficient towards acid conditions, i.e. chlorites can be separated into the alkaline species $MgOH^+$, $Al(OH)_4^-$ and $H_3SiO_4^-$ without significant change of the H^+ activity. In other words, in contrast to the other clay minerals in Valanginian marl, chlorites are much more stable under alkaline conditions.

In summary, the dissolution of quartz and clay minerals at high pH are proton producing which leads to a drop in pH. From these simple examples it is apparent that the speciation of the aqueous solution plays an important role in determining the properties of a given hydrolysis reaction.

5 NUMERICAL CALCULATION OF MARL ALTERATION

The highly simplified flow geometry on which the numerical calculations presented in this section are based is depicted in Fig. 3. The model used here focuses mainly on the major mineralogical alteration processes of the host rock surrounding the near-field. As shown schematically in Fig. 3, groundwater assumed to be in equilibrium with the marl infiltrates into the repository indicated by the cement zone, and then returns to the marl after reacting with various cement minerals such as portlandite, CSH-phases, ettringite and katoite (hydrogarnet). The emerging fluid has a pH which can range between approximately 12.5 to over 13 depending on the composition of the cement and a relatively low silica concentration ($\sim 10^{-5}$ M). It is no longer in equilibrium with the marl which begins to dissolve on immediate contact with the cement-reacted fluid.

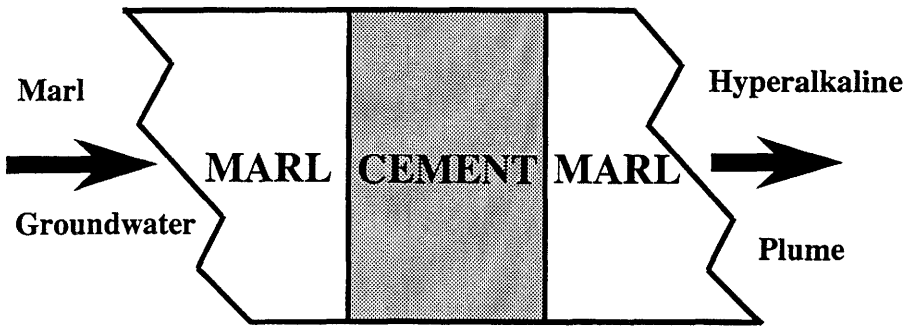

Figure 3: Schematic illustration showing the infiltration of groundwater from the surrounding marl host rock through a cement based radioactive waste repository and returning to the marl host rock.

This study does not describe the alteration of the cementitious repository near-field caused by transport of the undisturbed marl groundwater into the cement body, both because of the more complex flow geometry associated with the repository and the complicated processes involved in cement degradation. This is potentially an important aspect of the cement-marl interaction, however, since, because of the extremely low pCO_2 of the cement pore fluid, calcite can be expected to precipitate in the cement pore spaces thereby reducing the porosity and permeability and hence transport through the cement. This may in turn affect the ability of the infiltrating

groundwater to come to equilibrium with the cement. Effects such as cation exchange and other surface complexation reactions are not considered in this study.

5.1 Time-Space Continuum Model of Mass Transport

To investigate the rate of migration of a hyperalkaline plume into a marl host rock it is necessary to describe quantitatively, both spatially and temporally, the transport of fluid and its chemical interaction with minerals. The description which follows is based on a kinetic formulation of mineral reaction rates. The model applies to pure advective fluid transport in a homogeneous porous medium. Mass transport equations are solved using the quasi–stationary state approximation, implemented in the computer code **MPATH** for pure advective transport in a single spatial dimension (Lichtner, 1988, 1992). The details of the methods used in the code are discussed by Lichtner (1992). This approximation enables integration of mass conservation equations for a multicomponent system over geological time spans taking into account the full chemistry of the system comparable to that used in closed system calculations. Application of the quasi-stationary state approximation to conditions of local equilibrium has been considered in detail by Lichtner (1991). Preliminary results applying the transport model to the cement-marl system have been presented by Eikenberg and Lichtner (1992).

For the jth solute species mass conservation equations in the quasi–stationary state approximation can be written in the form

$$u\frac{d\Psi_j}{dx}(x;\,t) \;=\; -\sum_m \nu_{jm} I_m(x;\,t), \tag{27}$$

which represents a reaction path in the space coordinate x and a particular time t, where u denotes the Darcy flow velocity, ν_{jm} represents the matrix of stoichiometric coefficients corresponding to a set of simultaneous heterogeneous reactions of the form

$$\sum_{j=1}^{N} \nu_{jm} \mathcal{A}_j \rightleftharpoons \mathcal{M}_m, \tag{28}$$

for aqueous species $\mathcal{A}_j$ and mineral $\mathcal{M}_m$, and I_m denotes the correspondingreaction rate. This form of mineral reactions is very general and includes mineral-mineral replacement reactions as a special case. The generalized concentration Ψ_j is defined by the expression

$$\Psi_j \;=\; C_j + \sum_i \nu_{ji} C_i, \tag{29}$$

where C_j refers to the concentration of the jth primary species and C_i denotes the concentration of the ith aqueous complex (Lichtner, 1985). The coefficients ν_{ji} refer to the stoichiometric coefficient of the jth primary species in the ith complex. The concentrations of aqueous complexes are assumed to be in local equilibrium along the fluid flow path determined by appropriate mass action equations.

The independent variable time t enters the transport equations as a parameter referring to the state of alteration of the rock at a particular point x in the porous medium. The alteration of the mth mineral obeys the mass transfer equation

$$\frac{\partial \phi_m}{\partial t}(x, t) = \bar{V}_m I_m(x, t), \tag{30}$$

where ϕ_m and $\bar{V}_m$ denote the mineral volume fraction and molar volume, respectively. Within the quasi-stationary state approximation this latter equation is integratedover a time step Δt at a fixed point x in space resulting in the explicit finite difference equation:

$$\phi_m(x, t + \Delta t) = \phi_m(x, t) + \Delta t \, \bar{V}_m I_m(x, t), \tag{31}$$

from which the mineral volume fraction at time $t + \Delta t$ is determined from its value at time t. By solving these equations repeatedly the time evolution of the system can be calculated.

To complete these equations it is necessary to specify appropriate initial and boundary conditions. These give the initial rock composition $\phi_m^\infty(x)$, and the composition of the infiltrating fluid at the inlet to the porous rock column $\Psi_j^0(t)$, specified by the equations

$$\phi_m(x, t = 0) = \phi_m^\infty(x), \tag{32}$$

and

$$\Psi_j(x = 0, t) = \Psi_j^0(t), \tag{33}$$

respectively. Because of the assumption of pure advective transport it is not necessary to specify the composition of initial fluid which is flushed from the system by the infiltrating fluid.

The solute transport equations are solved sequentially with the mineral mass transfer equations taking into account the alteration of the host rock over the time step Δt. This approach in which the solution composition is weakly coupled to the mineral abundances is referred to as a multiple reaction path model (Lichtner, 1988, 1992). Because the quasi-stationary state approximation allows macroscopic time steps Δt to be used which are not restricted by stability

requirements as in usual finite difference schemes, these equations can be integrated over millions of years for multicomponent systems with virtually an unlimited number of reacting species in reasonable cpu times on modern workstations.

In the present formulation changes in porosity and permeability are not coupled to the flow equations. Nevertheless, once a solution has been obtained changes in porosity can be calculated as a function of time and distance along the flow path from the equation

$$\phi(x, t) = 1 - \sum_m \phi_m(x, t). \tag{34}$$

Zero or even negative values of the porosity are possible from this equation. In such cases coupling porosity changes to the flow equations would lead to complete blocking of the flow path and flow would cease. This is, however, only one of a range of possibilities. At the other extreme, it is conceivable that mechanical forces acting on the rock keep the flow path open. Regardless of which situation actually occurs, the results of calculations presented here give an indication of the possible conditions to expect and should not necessarily be interpreted literally. Certainly the calculations provide an estimate of the time when flow would cease if the flow path were to be completely blocked by mineral alteration products.

5.2 Kinetic Formulation of Mineral Reaction Rates

The kinetic rate law used in the present calculations has the form (Aagaard and Helgeson, 1983):

$$I_m = -k_m s_m \left(1 - \mathrm{e}^{-\mathbf{A}_m/RT}\right), \tag{35}$$

where I_m denotes the reaction rate of the mth mineral in units of moles per unit volume per unit time, k_m refers to the rate constant, s_m designates the specific surface area in units of area per unit volume of bulk porous medium, $\mathbf{A}_m$ denotes the chemical affinity of the overall hydrolysis reaction, and R and T indicate the gas constant and temperature, respectively. The reaction rate represents an average value taken over a representative elemental volume (REV) containing many mineral grains. As defined, the rate is positive for precipitation and negative for dissolution. An important feature of this form of the rate law is the quantity in brackets, referred to as the affinity factor, which allows the rate to vanish at equilibrium as it must.

Kinetic rate constants k_m for silicate minerals are observed to increase with increasing pH

(Brady and Walther, 1989). These authors obtained the phenomenological relation

$$\log k_m = \log k_m^0 + \beta(\mathrm{pH} - \mathrm{pH}_0), \tag{36}$$

for $\mathrm{pH} \geq \mathrm{pH}_0$, valid at 25°C. The rate constant k_m^0 corresponds to the threshold $\mathrm{pH}_0 \simeq 8$ and the slope $\beta \simeq 0.3$ also applies for 25°C. Thus the kinetic rate constant is approximately 1.35 log units larger at pH 12.5 compared to its value at pH 8 at 25°C. For higher temperatures the rate constant increases even more rapidly with increasing temperature. For example, at 70°C, Brady and Walther (1989) report a slope of approximately $\beta \simeq 0.5$. This would result in an enormous increase in the rate constant by 2.25 log units from pH 8 to 12.5.

5.2.1 Scaling Relations

For very long time spans the solution to the transport equations becomes insensitive to the values chosen for the rate constants k_m (Lichtner, 1993). In this case, the solution to the transport equations may always be related to the local equilibrium limit by scaling the time and space coordinates of the kinetic solution (Lichtner, 1993). In this sense the rate expression is referred to as a pseudo-kinetic rate law, because although it may not take into account the detailed reaction mechanism, nevertheless, it allows deviations from equilibrium to be investigated. To ascertain the uncertainty of the solution to the mass transport equations on the kinetic rate constants, mineral surface areas, and Darcy flow velocity it is useful to consider the scaling relations obtained by multiplying the rate constants by the same factor σ and the Darcy flow velocity by a factor σ'. Then the solution $C(x, t; \{k\}, u)$ to the transport equations, in the absence of any inherent length scale in the system, obeys the scaling relation

$$C(x, t; \sigma\{k\}, \sigma' u) = C(\frac{\sigma}{\sigma'}x, \sigma t; \{k\}, u), \tag{37}$$

for arbitrarily chosen scale factors σ, σ', where the notation $\{k\} = \{k_1, k_2, \cdots\}$ with $\sigma\{k\} = \{\sigma k_1, \sigma k_2, \cdots\}$ is used. A similar relation exists for the mineral volume fractions $\phi_m(x, t; \{k\}, u)$. This relation enables a solution belonging to a different Darcy flow velocity $\sigma' u$, and different kinetic rate constants $\sigma\{k\}$, to be obtained from the original solution with Darcy velocity u and rate constants $\{k\}$.

Taking $\sigma' = 1$ leads to a relation in which only the rate constants are scaled:

$$C(x, t; \sigma\{k\}, u) = C(\sigma x, \sigma t; \{k\}, u). \tag{38}$$

According to this relation, scaling the rate constants by the same factor σ is equivalent to scaling the time and space coordinates of the original solution by the same factor. The consequences of this relation has been discussed extensively by Lichtner (1993), and forms the basis for understanding the local equilibrium limit. Two additional relationships can be found by setting $\sigma = 1$ and taking $\sigma' = \sigma$. This leads to the identities

$$C(x, t; \{k\}, \sigma' u) = C(\frac{1}{\sigma'}x, t; \{k\}, u), \tag{39}$$

and

$$C(x, t; \sigma\{k\}, \sigma u) = C(x, \sigma t; \{k\}, u), \tag{40}$$

respectively. According to the first of these relations doubling the fluid velocity with identical rate constants halves the distance for a given time t. The second relation says that doubling both the kinetic rate constants and fluid velocity by the same factor is equivalent to doubling the time coordinate of the original solution without changing the space coordinate.

5.2.2 Homogeneous and Fractured Porous Medium

In a homogeneous porous medium in which the mth mineral grain is idealized as a cube of length b_m, the specific surface area of the mineral is given by

$$s_m = \frac{6}{b_m}\phi_m. \tag{41}$$

By comparison for transport along a fracture with aperture w, the specific surface area of a mineral contained in the wall rock is equal to

$$s_m = \frac{2}{w}\phi_m, \tag{42}$$

where in this case ϕ_m represents the volume fraction of the mth mineral at the surface of the wall rock.

The calculation for a porous medium may be related to that corresponding to flow through a simple parallel plate fracture by scaling the kinetic rate constants by the ratio of the mineral surface area for the fracture to the surface area in the porous medium. Denoting this ratio by σ, it is equal to

$$\sigma = \frac{b_m}{3w}, \tag{43}$$

as follows from Eqns.(41) and (42). For a typical grain size one tenth the fracture aperture

$$\sigma \sim 1/30. \tag{44}$$

Using this value for σ it follows that reaction fronts would be displaced by a factor 30 for transport in a fracture from the corresponding porous medium result, assuming the same Darcy flow velocities. Actually the situation is more complicated than this because of the differing permeabilities corresponding to the fracture network and rock matrix.

5.3 Physicochemical Input Parameters

5.3.1 Cement Pore Water Inlet Composition

Three distinct cement-equilibrated inlet pore waters are considered. The first two solutions are derived from the $NaHCO_3$– and NaCl–type groundwaters with compositions as presented in Table 6. The ions Na^+ and K^+ in the marl groundwater are assumed to percolate without change in concentration through the cement and thus are not controlled by mineral solubilities. This neglects the slow release of alkalies from the cement as it degrades with time which the third solution attempts to take into account. The inlet water composition for all three cases is derived from equilibrium with eight minerals: portlandite, brucite, calcite, katoite, foshagite, ettringite, goethite, and friedel salt. The minerals katoite (an endmember of the hydrogrossular series C_3AS_3–C_3AH_3, see Lager et al., 1989) and foshagite are treated as model solids representing aged calcium silicate and aluminate phases in "old" cement, indicative of a gradual degradation of the repository over thousands of years. The concentration of Cl^- is controlled by equilibrium with friedel salt which was found to be supersaturated at high pH using the chloride concentrations of the original marl groundwater. In addition, due to the relatively high concentrations of Ca^{2+}, SO_4^{2-} and F^-, but extremely low CO_2 partial pressure in cement, precipitation of secondary minerals strontianite and fluorite is expected to occur in the cement, and hence these phases are assumed to control the concentrations of strontium and fluoride. The pH is determined by charge balance and the redox potential by equilibrium with pyrite present in the marl. This gives a complete set of equations (14 = 8+2+2+1+1) to determine an equal number of unknowns given by the concentration of the species: K^+, Na^+, Ca^{2+}, Mg^{2+}, Fe^{2+}, Sr^{2+}, Al^{3+}, $SiO_{2(aq)}$, SO_4^{2-}, CO_3^{2-}, F^-, Cl^-, and the Eh and pH.

Table 6: Inlet cement equilibrated pore-water solutions derived from NaCl– and $NaHCO_3$–type groundwaters used in the theoretical calculations.

	Cement–pore water (total concentrations [mol/l])	
	NaCl–derived	$NaHCO_3$–derived
Na^+	1.78×10^{-1}	1.83×10^{-2}
K^+	3.32×10^{-4}	1.02×10^{-4}
Ca^{2+}	2.78×10^{-2}	1.57×10^{-2}
Mg^{2+}	4.34×10^{-9}	1.48×10^{-8}
Sr^{2+}	1.21×10^{-4}	8.78×10^{-5}
$Al(OH)_4^-$	2.47×10^{-5}	6.04×10^{-6}
$Fe(OH)_4^-$	1.31×10^{-8}	3.71×10^{-9}
$C_{(tot)}{}^a$	2.27×10^{-5}	1.36×10^{-6}
$Si_{(tot)}{}^b$	1.05×10^{-5}	7.09×10^{-6}
SO_4^{2-}	5.84×10^{-3}	6.19×10^{-4}
F^-	5.55×10^{-5}	1.57×10^{-4}
Cl^{-c}	3.07×10^{-3}	8.52×10^{-4}
T[°C]	25	25
I[M]	0.179	0.059
pH	13.05	12.54
Eh [mV]	−624.1	−594.0
log pCO_2[bar]	−13.18	−13.18

[a] $C_{(tot)} = H_2CO_3 + HCO_3^- + CO_3^{2-}$

[b] $Si_{(tot)} = SiO_{2(aq)} + H_3SiO_4^- + H_2SiO_4^{2-} + CaH_2SiO_4$

[c] Concentration obtained by equilibration with Friedel Salt.

Comparison of Tables 6 and 4 show several significant differences between the $NaHCO_3$– and NaCl–type marl groundwaters and the corresponding cement equilibrated pore solutions. Besides a much higher pH compared to the undisturbed marl groundwater, the cement solutions have a much lower pCO_2 and total silica concentration. The Cl^- ion has a much lower concentration in the cement pore solutions than in the marl because of the solubility control by friedel salt. The cement equilibrated NaCl–derived groundwater has a much higher pH

than the corresponding $NaHCO_3$–derived groundwater. This may be attributed to the larger concentration of Na^+ in the NaCl–derived groundwater. In addition it is almost a factor of two higher in the concentration of calcium, a factor five higher in aluminum, almost a factor of twenty larger in carbonate, and a factor 10 higher in sulfate concentration.

5.3.2 Alkali Release

The third solution considered attempts in an empirical way to account for the release of alkalies during the early degradation of the cement through a time varing inlet concentration. At early times the high pH release is dominated by the hydroxides NaOH and KOH, rather than portlandite assumed for the first two solutions. Future modeling exercises should also consider the evolution of cement degradation implementing the most important incongruent phase reactions of typical cement systems to account for changes in the C/S–ratio of the cement with time.

The alkalies are present in cement in the form of solid solutions with readily-soluble sulfates and as minor constituents with clinker phases alite, belite, aluminate, and ferrite. Considerable uncertainty exists in understanding the release of alkali from a cementitious body with time. The leaching mechanism is believed to occur by diffusive transport across an alteration layer surrounding the K, Na-bearing phases. Thus the system is not in equilibrium and solubility constraints are not operable for K and Na. At present it is not possible to predict with certainty the partitioning of alkalies between solid and liquid phases. Therefore an empirical approach must be used to describe the release of alkalies as the cement degrades with time.

It is assumed that as marl groundwater flows through the cementitious repository leaching alkalies from the cement, the concentration of alkali in solution decreases exponentially with time according to a first order rate law as the inventory of alkalies in the cement is depleted. Thus the total alkali concentration in the cement pore solution $\Psi_j^0(t)$ is assumed to obey the expression

$$\Psi_j^0(t) = \left(\widehat{\Psi}_j^0 - \Psi_j^{gw}\right) e^{-\lambda_j t} + \Psi_j^{gw}, \tag{45}$$

with j = Na, K, where $\widehat{\Psi}_j^0$ represents the initial cement pore solution composition, Ψ_j^{gw} represents the ambient marl groundwater concentration, and λ_j denotes the decay time constant. According to this expression the total concentration of the alkali decays exponentially with time from the

initial value $\widehat{\Psi}_j^0$ to the ambient groundwater concentration Ψ_j^{gw} with a half-life τ_j given by

$$\tau_j = \lambda_j^{-1} \ln 2. \tag{46}$$

The pH of the resulting solution is calculated by equilibrating the solution at each instant in time with the same minerals used for the calcium hydroxide solution described above.

For conditions of pure advective transport with Darcy velocity u the flux of solute species flowing from the repository is equal to

$$\Omega_j = u\Psi_j^0(t), \tag{47}$$

and that entering the repository is postulated as

$$\Omega_j^{gw} = u\Psi_j^{gw}. \tag{48}$$

Integrating the difference in these quantities over time gives the total mass of the jth alkali leached from the cement as

$$\begin{aligned} M_j(t) &= W_j A \int_0^t \left[\Omega_j(t') - \Omega_j^{gw}\right] dt', \\ &= W_j \frac{uA}{\lambda_j} \left(\widehat{\Psi}_j^0 - \Psi_j^{gw}\right) \left[1 - \mathrm{e}^{-\lambda_j t}\right], \end{aligned} \tag{49}$$

where A denotes the cross-sectional area of the flow, and W_j represents the gram-formula-weight of the jth species. Letting $t \to \infty$, gives the initial inventory of alkali in the cement denoted by M_j^0:

$$M_j^0 = W_j \frac{uA}{\lambda_j} \left(\widehat{\Psi}_j^0 - \Psi_j^{gw}\right). \tag{50}$$

By taking the ratio of the initial inventories, an expression is obtained for the ratio of the decay constants given by

$$\frac{\lambda_{\mathrm{Na}}}{\lambda_{\mathrm{K}}} = \frac{M_{\mathrm{Na}}^0}{M_{\mathrm{K}}^0} \frac{W_{\mathrm{K}}}{W_{\mathrm{Na}}} \frac{\left(\widehat{\Psi}_{\mathrm{K}}^0 - \Psi_{\mathrm{K}}^{gw}\right)}{\left(\widehat{\Psi}_{\mathrm{Na}}^0 - \Psi_{\mathrm{Na}}^{gw}\right)}. \tag{51}$$

To determine values for the decay constants λ_{Na} and λ_{K} it is assumed that the mass ratio Na:K in the cement is 1:10, and the molar ratio in the pore solution is 1:2 (Berner, 1990). If an arbitrary value for $\lambda_{\mathrm{Na}} = 10^{-2}$ y^{-1} is selected yielding a half-life of approximately 69.3 years, this gives $\lambda_{\mathrm{K}} = 0.0034$ y^{-1} or a half-life of approximately 203.8 years. Other than the concentrations of K^+ and Na^+, the concentrations of the remaining species are fixed by the same solubility constraints as with the $NaHCO_3$– and NaCl–derived waters.

5.3.3 Mineralogical Composition of Marl

As stated above, the marl under investigation is composed mineralogically of essentially carbonates (mainly in form of calcite) aluminosilicates (clay minerals) and quartz. Because of the lack of reliable thermodynamic data, muscovite is chosen here to represent the rather complex illite, illite–smectite assemblage, and the crystallographically similar carbonate mineral dolomite ($CaMg(CO_3)_2$) is used instead of the carbonate mineral ankerite, a solid solution between the endmembers $CaCO_3$–$Fe^{II}CO_3$. Similar uncertainties also exist for the stoichiometrically complex group of chlorite minerals. Because the chlorite present in the host rock sediments is Fe-rich, 14-A daphnite is used to represent chlorite. The average modal composition of the host rock used in the numerical calculations corresponds to that given in Table 3.

5.3.4 Flow Conditions

As shown schematically in Fig 3, fluid equilibrated with cement is allowed to infiltrate from the repository into an unaltered Valanginian marl host rock. Calculations are carried out in a single spatial dimension for pure advective transport assuming a constant reference Darcy flow velocity of 1 m y^{-1} and constant porosity. Due to the assumption of pure advective transport (plug flow), mixing of cement–equilibrated and marl water at the front of the migrating plume does not take place. It is assumed that there is a sufficient quantity of cement to produce a hyperalkaline plume for tens of thousands of years. This is not an unreasonable assumption. Assuming flow to take place through a cross-sectional area of one square meter with a flow velocity of 1 m y^{-1} with a dissolved total calcium concentration of 2.5×10^{-2} moles $liter^{-1}$, then if all calcium comes from dissolution of portlandite in the cement this requires a mass of portlandite of approximately 10 metric tons for a leaching time of ten thousand years. A typical low-level nuclear waste repository may contain as much as several hundred thousand tons of cement (Berner, 1990).

5.3.5 Thermodynamic and Kinetic Data

The thermodynamic data used in the calculations were taken from the EQ3/6 computer package (Wolery, 1992) data base version R16, with the exceptions noted below. For portlandite a log

$K = -5.15$ corresponding to the reaction

$$Ca(OH)_{2(s)} \rightleftharpoons Ca^{2+} + 2\,OH^{-}, \tag{52}$$

was used. For ettringite a log K of 56.34 was used taken from Reardon (1992) corresponding to the reaction

$$Ca_6Al_2(SO_4)_3(OH)_{12} \cdot 26H_2O + 12\,H^{+} \rightleftharpoons 6\,Ca^{2+} + 2\,Al^{3+} + 3\,SO_4^{2-} + 26\,H_2O. \tag{53}$$

This is four orders of magnitude smaller compared to the value of 60.81 for the ettringite log K in the EQ3/6 data base and leads to a more reasonable sulfate concentration in the inlet fluid after equilibration with ettringite. A molar volume for ettringite of 701.175 cm^3 $mole^{-1}$ was also used in the calculations. For friedel salt a log K of 68.66 (Reardon, 1992) was used corresponding to the reaction

$$3CaO \cdot Al_2O_3 \cdot CaCl_2 \cdot 10H_2O + 12\,H^{+} \rightleftharpoons 4\,Ca^{2+} + 2\,Al^{3+} + 2\,Cl^{-} + 16\,H_2O, \tag{54}$$

with a molar volume of 296.7 cm^3 $mole^{-1}$.

Because of the paucity of kinetic data available for most of the minerals encountered in this study, as well as the large uncertainty in mineral surface areas, a single value of 1×10^{-15} moles cm^{-2} s^{-1} was used for the effective rate constant for all minerals with the exception of calcite, dolomite and daphnite for which a value of 5×10^{-15} moles cm^{-2} s^{-1} was used. This rate corresponds to an equilibration length on the order of a few meters for calcite, for example, with a Darcy flow velocity of 1 m y^{-1}. As noted above, for long time spans the results are insensitive to the values chosen for the rate constants. This is not the case for short time spans, however, in which case the mineral zone sequence and variation of fluid composition with time and distance may depend strongly on the choice of rate constants. It should be noted further that by scaling the rate constants by the same factor, although the solution composition and mineral alteration zones do not change, the time-distance relationships become altered and therefore it is not possible to assign an absolute time unless the rate constants and mineral surface areas are known more precisely.

5.4 Results

5.4.1 pH-Front Propagation

In Fig. 4a the calculated propagation of the pH–front is plotted as function of the logarithm of the distance from the repository for times of 500, 5,000, and 10,000 years for the $NaHCO_3$–derived water, and in Fig. 4b for the NaCl–derived water for times of 500, 2,000, 5,000 and 10,000 years. Note that because of changes in porosity during the simulations (section 5.4.3), there may be considerable uncertainty with regard to absolute values of the distance–time relations shown in Fig. 4 (and Figs. 5-10). However, the calculations are useful to demonstrate "worse case" scenarios for the migration of cement pore fluids. Different profiles are obtained corresponding to the two different water types. The NaCl water, because of its higher inlet pH, leads to a more aggressive advance of the pH plume. The pH is slightly more neutralized in this case compared to the $NaHCO_3$–derived water. The pH profile has a pronounced shoulder at a pH of approximately 12, especially visible for the NaCl-type groundwater, determined by various CSH-phases.

The high pH–front propagates at a retarded velocity compared to the fluid velocity. The retarded velocity varies greatly depending on the inlet fluid composition. For instance, after 5,000 years the original inlet fluid has traversed a distance of $\sim 5 \times 10^4$ m assuming a constant porosity of 10% resulting in an average pore fluid velocity $v = u/\phi = 10\,\mathrm{m\,y^{-1}}$. However, during this time the extension of the pH–front with values above 12 is approximately 100 m from the repository for the $NaHCO_3$–derived water, and 1,000 m for the NaCl–derived water. Hence the hyperalkaline plume is calculated to propagate with a speed of approximately 50 to 500 times less than that of the infiltrating groundwater. The pH–front travels with a relatively steep gradient into the geosphere, although note the log scale. The strong pH–neutralization effect of the host rock can be explained by the pH controlling hydrolysis reactions of aluminosilicates and quartz (see Eqns.(19)–(26)).

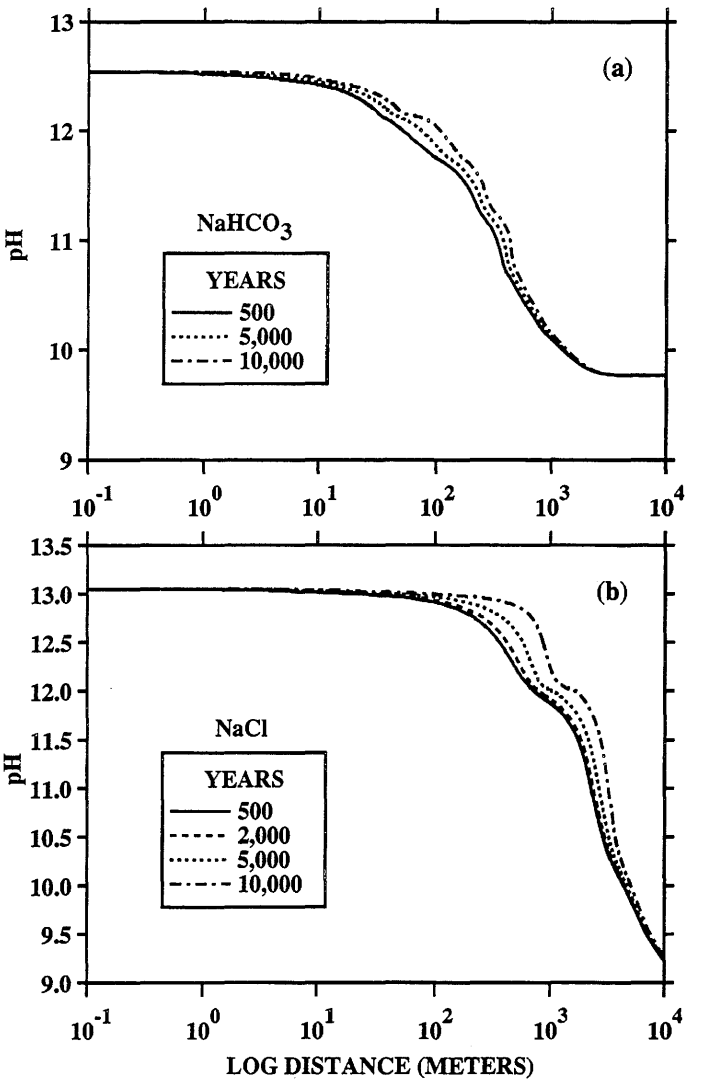

Figure 4: Propagation of the pH–front into Cretaceous Valanginian marl with time for infiltration of (a) $NaHCO_3$–derived water, and (b) NaCl–derived water. The different curves give the pH profile plotted as a function of the logarithm of distance in meters for times indicated in the figure. Note that an additional front not shown in the figure occurs further downstream, referred to as a salinity wave, where the inlet fluid comes in contact with the original marl groundwater.

5.4.2 Mineralogical Changes Along Flow Path

The fractional volume changes along the flow path of the primary and secondary mineral assemblages are presented in Fig. 5(a, b, c) for the $NaHCO_3$–derived water and in Fig. 6(a, b,

c) for the NaCl–derived water at an elapsed time of 10,000 years. The abbreviations of mineral names used in the figure are given in Table 7. Figures 5, 6(a) show the volume fraction profiles for the primary minerals and Figs. 5, 6(b, c) for secondary minerals. Near the cement–marl contact minerals ettringite, foshagite, friedel salt, katoite, goethite and brucite precipitate. This region is characterized by pH values of 12 and above. Goethite forms from dissolution of daphnite. Brucite and calcite replace dolomite.

Table 7: Mineral name abbreviations and their chemical formulae.

primary minerals			secondary minerals		
mineral	label	chem. formula	mineral	label	chem. formula
calcite	Cc	$CaCO_3$	hillebrandite	Hil	$Ca_2SiO_3(OH)_2 \cdot 0.17H_2O$
dolomite	Dol	$CaMg(CO_3)_2$	tobermorite	Tbm	$Ca_5Si_6H_{21}O_{27.5}$
quartz	Qtz	SiO_2	foshagite	Fos	$Ca_4Si_3O_9(OH)_2 \cdot 0.5H_2O$
pyrite	Py	FeS_2	katoite	Kat	$Ca_3Al_2(OH)_{12}$
muscovite	Mus	$KAl_3Si_3O_{10}(OH)_2$	ettringite	Etg	$Ca_6Al_2(SO_4)_3(OH)_{12} \cdot 26H_2O$
daphnite	Dph	$Fe_5Al_2Si_3O_{10}(OH)_8$	gibbsite	Gbs	$Al(OH)_3$
portlandite	Port	$Ca(OH)_2$	sepiolite	Sep	$Mg_4Si_6O_{15}(OH)_2 \cdot 6H_2O$
			brucite	Bru	$Mg(OH)_2$
			K-feldspar	Kfs	$KAlSi_3O_8$
			albite	Ab	$NaAlSi_3O_8$
			analcime	Anl	$Na_{0.96}Al_{0.96}Si_{2.04}O_6 \cdot H_2O$
			goethite	Goe	FeOOH
			friedel salt	Frl	$3CaO \cdot Al_2O_3 \cdot CaCl_2 \cdot 10H_2O$

For the $NaHCO_3$–derived water further downstream as the pH begins to drop to lower values gibbsite precipitates followed by overlapping zones of sepiolite, k-feldspar, analcime and finally albite. Gibbsite does not form with the NaCl-derived groundwater. Nevertheless, the profiles for the two waters are very similar in spite of the differing inlet solution compositions.

From these figures roughly four distinct reaction zones can be discerned. In the first zone bordering the repository and extending up to the daphnite dissolution front (0–10 m), the primary marl mineral assemblage is strongly altered and replaced completely by goethite, brucite, calcite, katoite (hydrogrossular), ettringite, and foshagite. In this zone the pH remains relatively constant equal to the value at the inlet with little or no neutralization. The second

zone is characterized by precipitation of feldspars and zeolites and occurs at a lower pH (~ 10). Finally in the third zone the fluid reaches equilibrium with the host rock minerals. The pH remains constant in this zone to where the injected fluid comes in contact with the original marl groundwater (not shown in the figure), referred to as a salinity wave. The salinity wave moves unretarded through the host rock.

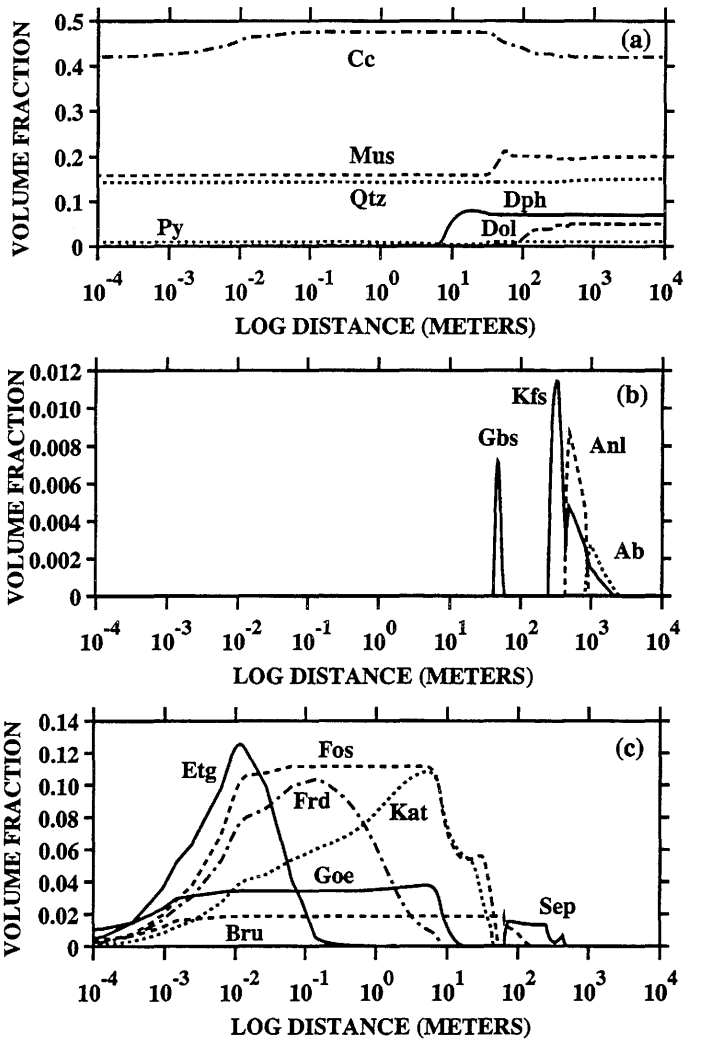

Figure 5: Mineral volume fractions of the primary marl assemblage (a) and secondary minerals (b, c) plotted as a function of the logarithm of the distance from the repository after an elapsed time of 10,000 years for the solid phase evolution resulting from the $NaHCO_3$ inlet solution. Note the different vertical scales for secondary minerals.

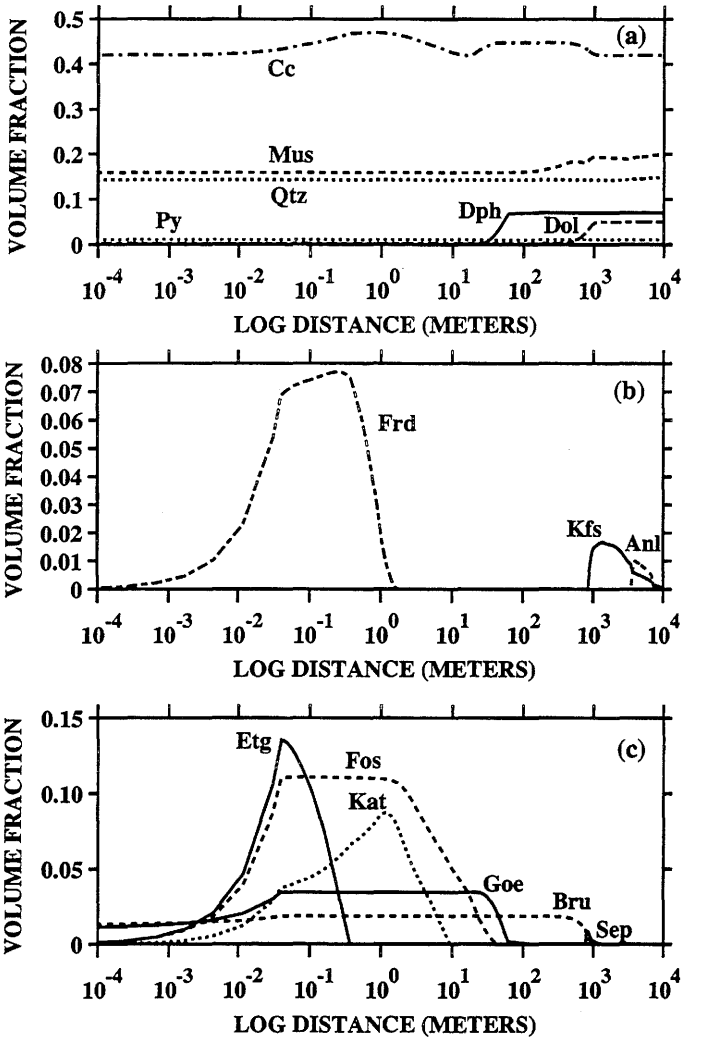

Figure 6: Mineral volume fractions of the primary marl assemblage (a) and secondary minerals (b, c) plotted as a function of the logarithm of the distance from the repository after an elapsed time of 10,000 years for the solid phase evolution resulting from the NaCl inlet solution. Note the different vertical scales for secondary minerals.

5.4.3 Porosity Changes Along Flow Path

The variation in porosity with time and distance is shown in Fig. 7. The porosity continually increases with time at the interface between the repository and the marl host rock as primary minerals dissolve. The zone of increasing porosity extends up to tens of centimeters from

the cement-marl contact into the marl. For times greater than approximately 5,000 years, the porosity becomes negative over a rather wide zone extending from several tens of centimeters from the cement-marl contact to tens of meters into the marl. In this region all available pore space is occupied by secondary mineral products. Although the calculation cannot be strictly correct for times longer than required for significant changes in porosity to take place, and especially for the occurrence of negative porosity, nevertheless it is still useful for showing the possible effects on the chemical evolution of infiltration of a high pH plume into marl host rock. In any case predicting the behavior of the system beyond the point where the porosity comes close to zero will be difficult.

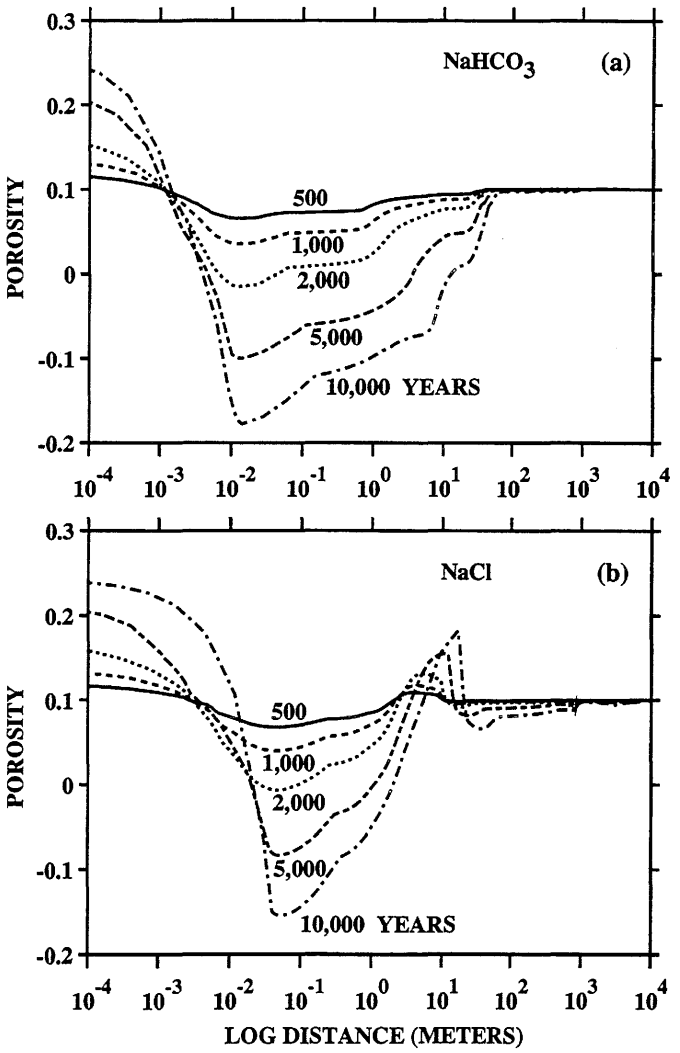

Figure 7: The evolution of porosity for infiltrating (a) $NaHCO_3$– and (b) NaCl–derived groundwaters plotted as a function of the logarithm of the distance at various times indicated in the figure.

5.4.4 Fluid Composition Changes Along Flow Path

The concentration of K–, Ca–, Si–, Al–, and Mg–bearing species are plotted as a function of the logarithm of the distance in Fig. 8 for the $NaHCO_3$–derived groundwater. Similar results are obtained for the NaCl-derived water and are, therefore, not discussed further. The dominant silica species in the region of high pH is the species CaH_2SiO_4 shown in Fig. 8(a). As the pH begins to drop, $H_3SiO_4^-$ becomes the dominant species (Fig. 8(b)). Finally the aqueous solution reaches equilibrium with quartz with equal concentrations of SiO_2 and $H_3SiO_4^-$. This latter property has apparently no deeper significance and is just coincidental, occurring at a unique pH of 9.8 in agreement with the calculated value (this does not occur for the NaCl water). The dominant calcium species over the entire pH range is Ca^{2+}. Its concentration decreases by approximately four orders of magnitude as the percolating fluid comes to equilibrium with the primary host rock minerals.

The concentration of the dominant aluminium and magnesium species are shown in Fig. 8(c). Apparently mineral reactions do not conserve aluminium within the solid phase under conditions of high pH to the same extent as for low pH conditions where the total aqueous aluminum concentration is considerably lower. The total aluminum concentration reaches a maximum of approximately 10^{-3} moles liter^{-1} and drops to below 10^{-6} moles liter^{-1} as the fluid comes to equilibrium with the host rock. The maximum in aluminium concentration is coincident with the daphnite dissolution front.

The precipitation of CSH-phases near the inlet in the high pH region has significant consequences on the silica activity of the aqueous solution. As shown in Fig. 8(b), as the pH drops in value there is a change of silica speciation from the Ca–Si complex $CaH_2SiO_{4(aq)}$ to silica hydrolysis products $H_3SiO_4^-$ and $SiO_{2(aq)}$. Because of the presence of less soluble CSH-phases near the cement–marl contact, the total silica activity remains low and SiO_2 hydrolysis products are well undersaturated. For this reason zeolites and feldspars remain undersaturated throughout this zone while gibbsite, for example, becomes supersaturated and precipitates.

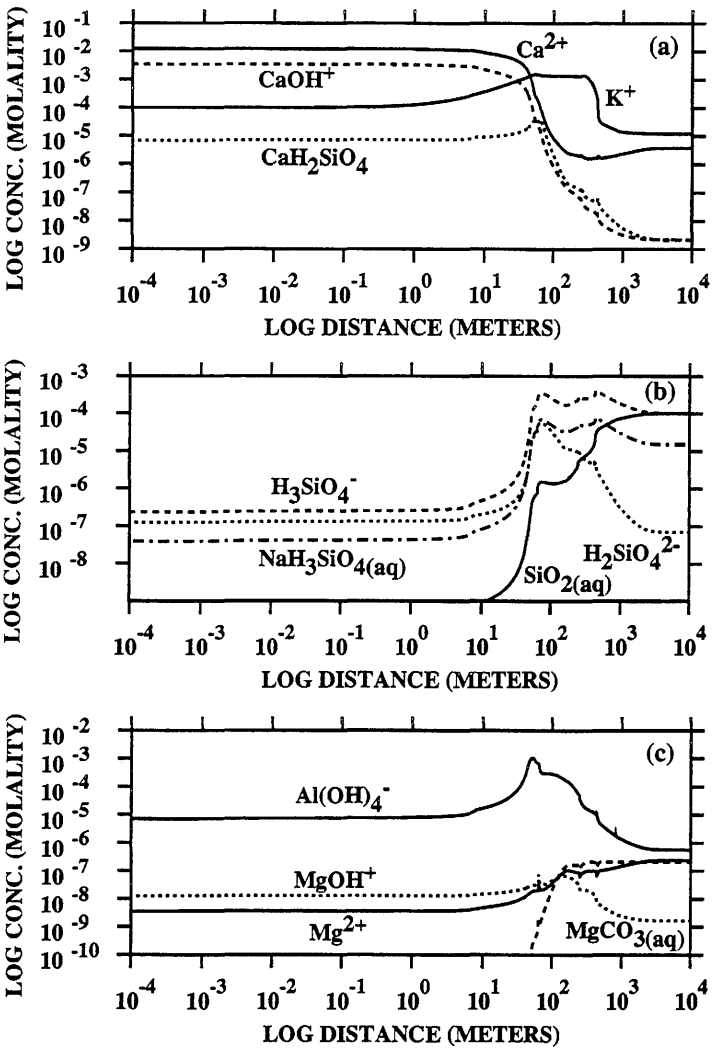

Figure 8: Solution composition for the $NaHCO_3$-derived inlet fluid for a selected set of species: (a) Ca, K, SiO_2–; (b) Na, SiO_2–; and (c) Mg, Al–bearing species plotted as a function of the logarithm of the distance for an elapsed time of 10,000 years.

5.4.5 Alkali Release

The third example involves the release of alkalies as a function of time. Pyrite is not included in this calculation as a primary mineral since it makes very little difference in the results. With the exception of species K^+ and Na^+, the same constraints are applied to determine the inlet fluid composition as in the $NaHCO_3$—derived groundwater. The inlet pH and concentrations of

species K^+, Na^+ and Ca^{2+} are plotted in Figs. 9a, b as a function of time. The pH drops from an initial value of approximately 13.25 to 12.57, consistent with the $NaHCO_3$—derived water, after approximately 1,000 years have elapsed.

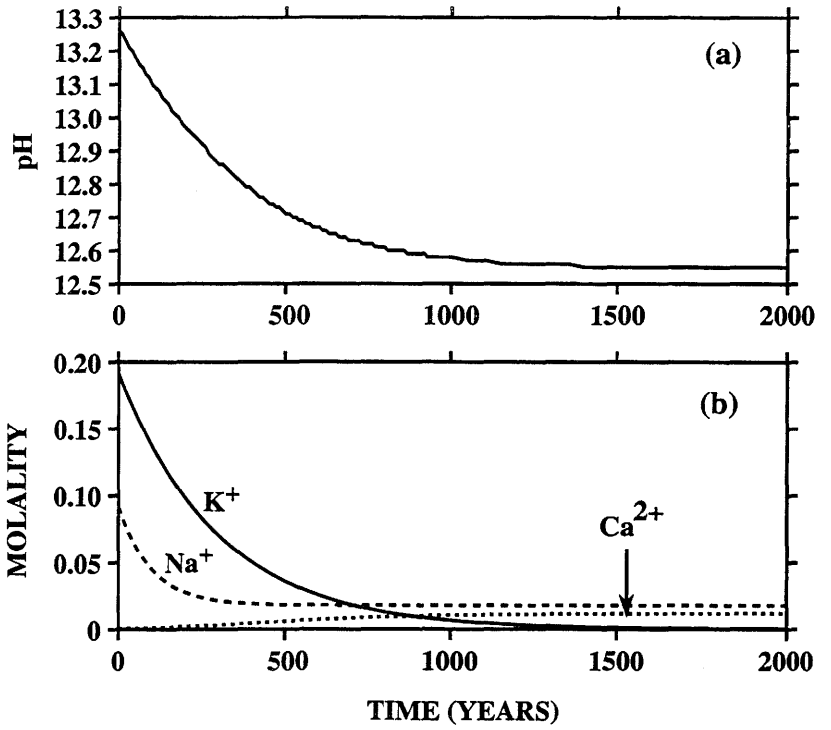

Figure 9: Time variation of: (a) pH, and (b) concentrations of species Na^+, K^+ and Ca^{2+}, for the alkali inlet solution assuming a decaying exponential release discussed in the text.

The pH and porosity profiles are shown in Figs. 10(a) and (b), respectively. The pH plume shows a more complicated behavior than in the $NaHCO_3$ case for earlier times, with the pH far from the repository increasing with time as the inlet pH drops. For long time spans the pH profile is similar to the $NaHCO_3$ case. The porosity profile is also similar to the $NaHCO_3$ case with somewhat greater dissolution occurring at the cement-marl contact. There is very little difference in the mineral modal abundances compared to the $NaHCO_3$-derived inlet fluid after an elapsed time of 10,000 years, and therefore these results are not presented.

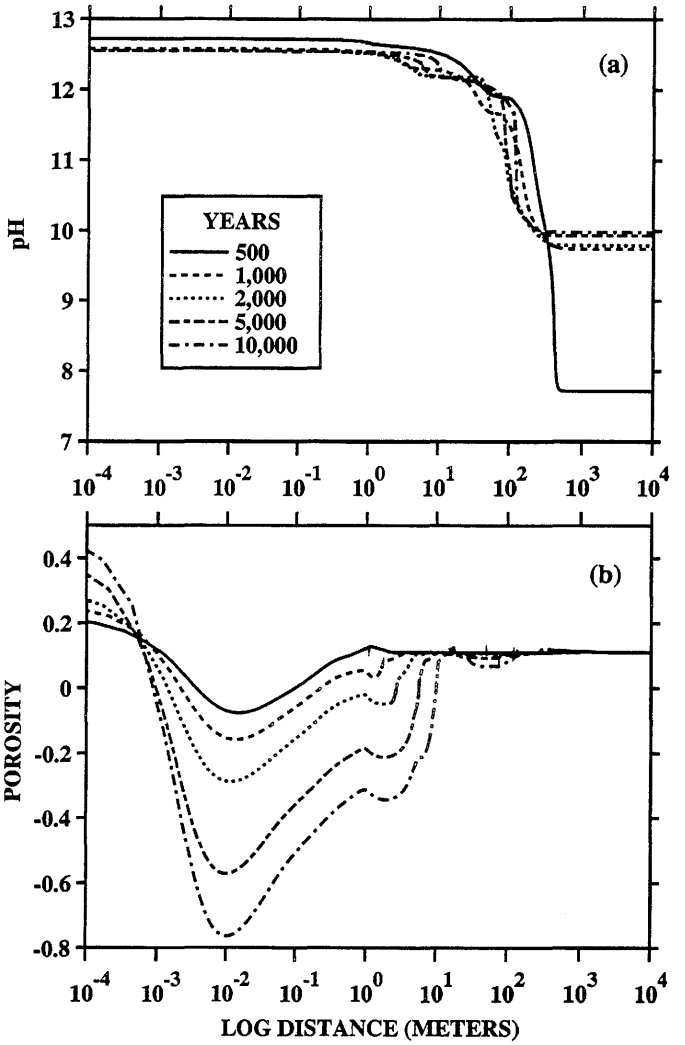

Figure 10: The evolution of pH and porosity for the alkali-release inlet solution plotted as a function of the logarithm of the distance at various times indicated in the figure.

5.4.6 Sensitivity to Kinetic Rate Constants

The sensitivity of the results on the choice of kinetic rate constants was investigated by varying separately the dissolution rates of the primary silicate minerals, the rates of secondary minerals, and the rate of calcite. The results were found to be most sensitive to the dissolution rates of the primary silicates whereas increasing the rate of calcite and secondary minerals had almost no effect on the results. The amount of secondary products foshagite, ettringite, katoite and friedel

salt that formed was found to be directly proportional to the dissolution rates of the silicate minerals, and hence these reactions control completely the time scale for porosity reduction in the marl. That the results were not sensitive to the precipitation rates of secondary minerals implies that the chosen rates were large enough to result in local equilibrium conditions. Recall that, according to Eqn.(35), the precipitation rate is equal to the rate constant multiplied by the affinity factor which increases with increasing disequilibrium. Thus even a relatively small value for the rate constant can result in a rate that rapidly becomes close to local equilibrium and therefore is independent of the kinetic rate constant and surface area.

6 DISCUSSION

One of the main results of this study, that near the cement-marl contact the porosity increases, whereas further downstream complete filling of all available pore space takes place, could have significant implications for transport in a fractured dominated flow system. The zone of high porosity created by dissolution of primary minerals at the cement-marl contact followed by sealing of the porous medium through precipitation of cement-type phases further downstream could, conceivably, result in channeling effects in a fracture controlled flow system. While it is difficult to apply the results of a single porosity system to transport in a fracture network, nevertheless such an extrapolation can be made for sufficiently rapid fluid flow within the fracture. In this case the fluid in the fracture is continuously flushed out with the hyperalkaline fluid, resulting in a constant fluid composition along the length of the fracture given by the inlet fluid emerging from the repository. The results of this study could then be applied to advective transport into the wall rock perpendicular to the fracture. Most likely, however, transport by diffusion rather than advection would dominate in this direction, and the results for pure advective transport are not strictly applicable.

It could be conjectured that diffusive transport between the fracture and wall-rock would result in formation of a low-permeable zone inside the wall-rock at a short distance from the fracture, thus sealing off further access of fluid in the fracture to the rock matrix. However, whether the fracture would in fact widen as a result of dissolution reactions, or close due to formation of secondary alteration products is not clear without actually performing the calculation. Near the repository the fracture would be expected to open, whereas further downstream it could eventually close. The fracture probably cannot close completely since once this would happen, undisturbed groundwater would redissolve the plug thereby opening the fracture. The fluid velocity would be expected to be an important factor in determining the distance from the repository where the fracture begins to close. The worse case scenario would be sealing off of the rock matrix to reaction with pore fluid in the fracture while keeping the fracture open, thus limiting the ability of the rock matrix to retard the migration of radionuclides and further neutralize the high-pH plume. This possibility needs to be addressed in future studies.

Finally, it should be emphasized that it is difficult to predict exactly the evolution of the detailed mineral paragenesis along the flow path as found in experiments and field observations. The reasons for this are due, in part, to (i) the short term duration of laboratory and field experiments (involving nucleation kinetic problems), (ii) natural analogue systems for which initial and boundary conditions, as well as flow conditions may be unknowable, (iii) the difficulty identifying amorphous phases and, (iv) the difficulty in predicting changes in porosity and permeability. Note, however, that because the pH neutralization capacity of the marl is determined mainly by dissolution of primary clay minerals and not by the sequence of mineral alteration products, the precise details of which secondary minerals form may not so important for predicting the propagation of the pH front. This can be of advantage when attempting to predict the speciation and solubilities of certain radionuclides released from a radioactive waste repository.

However, a word of caution is in order in interpreting the results of the simplified calculations in terms of flow evolution with time, because changes in material properties to flow and transport was not coupled in this work. Nevertheless, it is still possible to compute the expected changes in porosity that would result from mineral reactions. If these changes are found to be small, then the neclect of coupling transport with changes in material properties is still justified. However, as the calculations presented here indicate, that significant changes in porosity (and hence permeability) are likely to occur over relatively short time spans, the calculations are not strictly valid.

7 SUMMARY AND CONCLUSION

The most significant factors in determining the qualitative behavior of mineral alteration resulting from interaction of a hyperalkaline plume with rock-forming silicate minerals are the high pH and low silica concentration associated with cement pore waters. As a consequence silicate minerals such as quartz, clays and feldspars are incompatible with portlandite, CASH-phases. Therefore silicates begin to dissolve as they encounter a high pH plume emanating from a cementitious repository. This has the consequence that in the immediate vicinity of the cement–host rock interface the porosity must increase. However, as the concentrations of silica and aluminum increase, CASH-phases eventually become supersaturated and begin to precipitate further away from the repository resulting in a decrease in porosity. Because of the large molar volumes of these phases, the porosity decreases very rapidly until eventually all available pore space is completely filled. This analysis assumes that the intrinsic porosity associated with secondary alteration minerals is zero. Non-zero porosity of the alteration products would allow transport processes to continue, however, in such a case even less space would be available to contain the secondary phases.

Infiltration of hyperalkaline pore waters from a cementitious radioactive waste repository into the surrounding host rock can be expected to alter strongly the primary mineral assemblage and hence cause significant changes in the physical and chemical properties to the host rock in the near and far-field region of the repository. Time–space continuum model calculations predict rapid migration of a hyperalkaline plume into surrounding marl host rock, reduced by a factor of only approximately 50–100 compared to the Darcy flow velocity. Strong alteration of the host rock results in the precipitation of secondary cement-type phases in the vicinity of the cement-marl contact. At the contact between the cement and marl the porosity is predicted to increase with time as clay minerals dissolve, thereby producing a highly permeable zone at the interface between the marl and cement barrier. Slightly downstream from this zone the porosity decreases, becoming zero as all available pore space is occupied by cement-type phases. The final pH is strongly neutralized to values between approximately 8 and 10 due to the dissolution of clay minerals and the precipitation of silicates such as feldspar and zeolites. The calculations presented here are, at best, uncertain to within an overall scale factor.

Future work must consider the effects of changes in porosity and permeability of the host rock resulting from infiltration of a hyperalkaline aqueous solution. Because of the large changes to be expected in these quantities it will be very difficult to describe quantitatively the behavior of the system with any degree of certainty. In particular the effect of different flow geometries on the alteration process needs to be investigated. A most unfavorable scenario would occur if transport of hyperalkaline fluid took place in fractures and had little or no access to the host rock. This might be caused by transport through calcite lined fractures, for example, or sealing of the host rock by diffusion into the wall-rock accompanied by precipitation of calcite and cement-type phases (Steefel and Lichtner, 1994). Perhaps the most significant result obtained from the model calculations is the *increase* in porosity in the immediate vicinity of the cement-marl contact, followed by a porosity *decrease* further from the contact. This result implies that reaction within the fracture could result in widening of the fracture, while reaction in the wall rock would seal off further access of the hyperalkaline fluid to clay minerals due to precipitation of cement-phases deeper within the wall rock resulting in channeling with the creation of preferential flow paths for transport of radionuclides. Clearly the presence of a hyperalkaline plume greatly complicates the safety assessment of a cementitious waste repository.

Finally the thermodynamic and kinetic data used in calculations such as these need to be refined. This includes, as well, in situ measurements of the mineral surface areas in contact with the fluid, especially for dissolution reactions involving primary silicate minerals which control the time and length scales of the alteration process. In addition the secondary alteration products which are likely to form need to be identified by experiments and evidence from natural systems. However, it is not expected that the main conclusion of this work, namely the large changes in porosity and permeability which accompany the alteration process and the spatial relation of increased porosity at the marl-cement contact followed by reduced porosity further away from the repository, will change.

8 ACKNOWLEDGMENTS

This study was stimulated by the NAGRA "Störeinflüsse" group (coordinator I. G. McKinley) which had the task of investigating geochemical disturbances in the near-field as well as in the geologic barrier around a repository for low and intermediate level radioactive waste. We wish to thank U. Berner (PSI) and M. Mazurek (Universität Bern) for their kind assistance of

providing auxiliary data and for fruitful discussions during this study. In addition we thank Ian McKinley, Carl Steefel, Russell Alexander and Tjerk Peters for helpful discussions and Dave Savage for his careful review.

9 REFERENCES

Aagaard, P. and Helgeson, H. C. (1983) Activity/composition relations among silicates and aqueous solutions: II. chemical and thermodynamic consequences of ideal mixing of atoms on homological sites in montmorillonites, illites and mixed–layer clays. *Clays Clay Min.* **31,** 207 – 217.

Alexander, W. R. (Ed.) (1992) A natural analogue study of cement pore waters and their interaction with a sedimentary host rock. *NAGRA Technical Report* **NTB 91-10.**

Alexander, G. B., Heston, W. M. and Iler, R. K. (1954) The solubility of amorphous silica in water. *J. Phys. Chem.* **58,** 453–455.

Atkinson, A., Hearne, J. A. and Knights, C. F. (1987) Aqueous chemistry and thermodynamic modeling of $CaO–SiO_2–H_2O$–gels. *AERE Report* **12548,** Harwell Laboratory, UK.

Atkins, M., Glasser, F. P., Kindness, A. and Macphee, D. E. (1991) Solubility data for cement hydrate phases. *GB:DOE Report No.:* DoE/HMIP/RR/91/032, 23pp.

Bennett, D. G., Read, D., Atkins, M., and Glasser, F. P. (1992) A thermodynamic model for blended cements. II: Cement hydrate phases; thermodynamic values and modeling studies. *J. Nucl. Mat.* **190,** 315–325.

Berner, U. R. (1987) Modeling pore water chemistry in hydrated cement. *Mat. Res. Soc. Symp. Proc.* **84,** 319–330.

Berner, U. R. (1990) A thermodynamic description of the evolution of pore water chemistry and uranium speciation during the degradation of cement. *PSI-Report* **62** and *Nagra Technical Report* **NTB 90-12.**

Brady, P. V. and Walther, J. V. (1989) Controls on silicate dissolution rates in neutral and basic pH solutions at 25°C. *Geochim. Cosmochim. Acta* **53,** 2823–2830.

Bryant, S. L., Schechter, R. S., and Lake, L. W. (1986) Interactions of precipitation/dissolution waves and ion exchange in flow through permeable media, *AIChE J.* **32,** 751–764.

Bunge, A. L., Klein, G., and Radke, C. J. (1980) Divalent ion exchange with alkali, *SPE* **8995,** *5th Int. Symp. Oilfield and Geothermal Chem.*, Stanford, May.

Bunge, A. L., and Radke, C. J. (1982) Migration of alkaline pulses in reservoir sands, *Soc. Pet. Eng. J.*, December, 998–1012.

Bunge, A. L., and Radke, C. J. (1983) Divalent ion exchange with alkali, *Soc. Pet. Eng. J.*, August, 657–668.

Bunge, A. L., and Radke, C. J. (1985) The origin of reversible hydroxide uptake on reservoir rock, *Soc. Pet. Eng. J.*, October, 711–718.

Busey, R. H. and Mesmer, R. E. (1977) Ionization equilibria of silicic acid and polysilicate formation in aqueous sodium chloride solutions to 300°C. *Inorg. Chem.* **16,** 2444-2450.

Chermak, J. A. and Lichtner, P. C. (1991) Low temperature transformations in shales: an experimental and modelling investigation. *EUG* **3,** p. 475.

Cooke, C. E. Jr., Williams, R. E., and Kolodzie, P. A. (1974) Oil recovery by alkaline water-flooding, *J. Pet. Tech.*, December, 1365–1374.

deZabala, E. F., Vislocky, J. M., Rubin, E., and Radke, C. J. (1982) A chemical theory for linear alkaline flooding, *Soc. Pet. Eng. J.*, April, 245–258.

Eikenberg, J. (1990) On the problem of silica solubility at high pH. *PSI Report* **74** and *NAGRA Technical Report* **NTB 90-36.**

Eikenberg, J. and Lichtner, P.C. (1992) Propagation of hyperalkaline cement pore waters into the geologic barrier surrounding a radioactive waste repository. In: Water-Rock Interaction (Kharaka and Maest, eds.) A.A. Balkema, Rotterdam, 377–380.

Ewart, F. T., Sharland, S. M. and Tasker, P. W. (1985) The chemistry of the nearfield environment. *Mat. Res. Soc. Symp. Proc.* **50,** 539 – 546.

Glasser, F. P., MacPhee, D. and Lachowski, E. E. (1988) Modeling approach to the prediction of equilibrium phase distribution in slag–cement blends and their solubility properties. *Mat. Res. Soc. Symp. Proc.* **112,** 3–12.

Goto, K. J. (1955) States of silica in aqueous solution. I. Polymerisation and depolymerisation. *J. Chem. Soc. Japan* **76,** 1364–1366.

Grauer, R. (1988) The corrosion behaviour of carbon steel in portland cement. *Nagra,* **NTB 88-02E.**

Greenberg, S. A. (1957) The depolymerisation of silica in sodium hydroxide solutions. *J. Am. Chem. Soc.* **61,** 960–965.

Greenberg, S. A. and Chang, T. N. (1965) Investigation of the hydrated calcium silicates II. Solubility relationships in the calcium oxide–silica–water system at 25°C. *J.Phys. Chem.* **69,** 1151–1173.

Greenberg, S. A. and Price, E. W. (1957) The solubility of silica in solutions of electrolytes. *J. Phys. Chem.* **61,** 960–965.

Haworth, A., Sharland, S. M., Tasker, P. W. and Tweed, C. J. (1987) Evolution of the groundwater chemistry around a nuclear waste repository. *Nirex Safety Assessment Report* **No. 111.**

Iler, R. K. (1979) *The chemistry of silica.* Wiley Interscience, New York.

Jefferies, N. L., Tweed, C. J. and Wisbey, S. J. (1988) The effect of changes in pH within a clay surrounding cementitious repository. *Mat. Res. Soc. Symp. Proc.* **112,** 43–52.

Jennings, H. Y. Jr., Johnson, C. E. Jr., and McAuliffe, C. D. (1974) A caustic waterflooding process for heavy oils, *J. Pet. Tech.*, December, 1344–1352.

Jensen, J. A., and Radke, C. J. (1988) Chromatographic transport of alkaline buffers through reservoir rock, *SPE Res. Eng.*, August, 849–856.

Johnston, R. M. and Miller, H. G. (1984a) The effect of pH on the stability of smectite. **AECL–8366.**

Johnston, R. M. and Miller, H. G. (1984b) Effect of pH on smectite stability. *In: Swedish Nuclear Fuel and Waste Management Company Technical Report* **SKB–KBS 84– 11.**

Kalousek, G. L. (1952) Application of differential thermal analysis in a study of the system lime–silica–water. *Proc. 3rd Int. Symp. on Chemistry of Cements,* London, p. 296.

Khoury, H. N. and Nassir, S. (1982) High–temperature mineralization in the bituminous limestone in Maqarin area – North Jordan. *N.Jb. Minr. Abh.* **144,** 197–213.

Khoury, H. N., Salameh, E. and Abdul–Jahr, Q. (1985) Characteristics of an unusual highly alkaline water from the Maqarin area, Northern Jordan. *J. Hydrol.* **81** 79–91.

Lager, G. A., Armbruster, Th., Rotella, F. J. and Rossman, G. R. (1989) OH-substitution in garnets: X-ray and neutron diffraction, infrared and geometric modeling studies. *Am. Min.* **74,** 840–851.

Lea, F. M. (1970) The chemistry of cement and concrete. *3rd Ed., Edward Arnold (Publishers) Ltd.,* 727pp.

Lichtner, P. C. (1985) Continuum model for simultaneous chemical reactions and mass transport in hydrothermal systems. *Geochimica et Cosmochimica Acta* **49,** 779–800.

Lichtner, P. C. (1988) The quasi-stationary state approximation to coupled mass transport and fluid-rock interaction in a porous medium. *Geochim. et Cosmochim. Acta* **52,** 143–165.

Lichtner, P. C. (1991) The quasi-stationary state approximation to fluid-rock interaction: local equilibrium revisited. *Advances in Physical Geochemistry (ed. in Ganguly,)* **72,** 454–562.

Lichtner, P. C. (1992) Time–space continuum description of fluid-rock interaction in permeable media, *Water Resources Research* **28,** 3135–3155.

Lichtner, P. C. (1993) Scaling properties of time–space kinetic mass transport equations and the local equilibrium limit. *Am. J. Sci.* **293,** 1–40.

Mallison, L. G. and Davies, I. C. (1987) A historical examination of concrete. *CEC Report* **EUR 10937 EN.**

March, A. R., Klein, G. and Vermeulen, T. (1975) Polymerisation kinetics and equilibria of silicic acid in aqueous systems. Lawrence Berkeley Laboratory report LBL-4415.

Mazurek, M. (1991) The interface between marl and concrete lining in the Seelisberg tunnel. *Nagra Unpublished Report.*

Milodowski, A. E., Pearce, J. M., Hughes, C. R., and Khoury, H. N. (1992) A preliminary mineralogical investigation of a natural analogue of cement–buffered hyperalkaline groundwater interaction with marl, Maqarin, Northern Jordan. British Geological Survey **Report WG/92/18C.**

Mungan, N. (1979) A review and evaluation of alkaline flooding, *Petroleum Recovery Inst.*, Applications Report AR-4, January.

Novosad, Z. and Novosad, J. (1984) The effect of hydrogen ion exchange on alkalinity loss in alkaline flooding. *Soc. Pet. Eng. J. February,* 49–52.

Reardon, E. J. (1992) Problems and approaches to the prediction of the chemical composition in cement/water systems. *Waste Management,* **12,** 221–239.

Sarkar, A. K., Barnes, M. W. and Roy, D. M. (1982) Longevity of borehole and shaft sealing materials: thermodynamic properties of cements and related phases applied to repository sealing. Office of Nuclear Waste Isolation, Technical Report **ONWI-201,** 52pp.

Savage, D., Huges, C. Milodowski, A. E., Bateman, K. Pearce, J. M., Rae, E. I. J. and Rochelle, C. A. (1990) The evaluation of chemical mass transfer in the disturbed zone of a deep geological disposal facility for radioactive wastes. I. Reaction of silicates with calcium hydroxide fluids. *UK Nirex Ltd Report* **NSS/R244.**

Savage, D., Bateman, K., Hill, P. I. Huges, C. Milodowski, A. E., K. Pearce, J. M., and Rochelle, C. A. (1991) The evaluation of chemical mass transfer in the disturbed zone of a deep geological disposal facility for radioactive wastes. II. Reaction of silicates with Na-K-Ca hydroxide fluids. *UK Nirex Ltd Report* **NSS/R283.**

Schwarzentruber, J., Fürst, W. and Renon, H. (1987) Dissolvation of quartz into dilute alkaline solutions at 90°C: a kinetic study. *Geochim. Cosmochim. Acta* **51,** 1867–1874.

Steefel, C. I. and Lichtner, P. C. (1994) Diffusion and reaction in rock matrix bordering a hyperalkaline fluid–filled fracture. *Geochim. et Cosmochim. Acta,* in press.

Sydansk, R. D. (1982) Elevated–temperature caustic/sandstone interaction: implications for improving oil recovery. *Soc. Pet. Eng. J.* August, 453–462.

Thomassin, J. H. and Rassineux, F. (1992) Ancient analogues of cement-based materials: stability of calcium silicate hydrates. *Applied Geochemistry* Suppl. Issue No. 1, 137–142.

Thornton, S. D. and Radke, C. J. (1988) Dissolution and condensation kinetics of silica in alkaline solution. *Soc. Pet. Eng. J.* May, 743–752.

Wolery, T. J. (1992) EQ3NR, a computer program for geochemical aqueous speciation-solubility calculations: user's guide and related documentation (version 7.0). Lawrence

Livermore National Laboratory, Livermore, CA, UCRL report **UCRL-MA-110662 PT III,** 246pp.